Available online at www.CivileJournal.org

Civil Engineering Journal

(E-ISSN: 2476-3055; ISSN: 2676-6957)

Vol. 11, No. 03, March, 2025

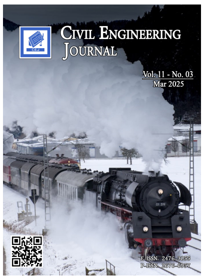

An Innovative Design of Strip and Circular Footings on Sand Surface: Stress–Density Framework

Mohamed I. Ramadan [1, 2] *

[1] *Assistant Professor, Faculty of Engineering-Rabigh, King Abdulaziz University, Jeddah, Saudi Arabia.*

[2] *Lecturer, Civil Engineering Department, Faculty of Engineering, Assiut University, Assiut, Egypt.*

Received 30 November 2024; Revised 03 February 2025; Accepted 11 February 2025; Published 01 March 2025

Abstract

The bearing capacity of shallow foundations subjected to vertical centric loads has been extensively investigated. Despite the variability in the bearing capacity factor $N\gamma$ as proposed by different methodologies, the classical solution remains dominant in design codes. Critical variables affecting the bearing capacity of sand encompass sand particle morphology, footing width or diameter (B or D), mean effective stress level (p'), and sand relative density (Dr). Different sand types may exhibit distinct mobilization friction angles (ϕ_m) at the same Dr and p', resulting in varied stress-strain behaviors. Thus, the actual bearing capacity may not be accurately reflected by estimates of $N\gamma$ derived from a constant peak friction angle (ϕ_p) value. In this study, a Three-Dimensional Finite Element Model (3D-FEM) has been applied to both strip and circular footings, employing a hypoplastic constitutive sand model to replicate sand behavior. The model efficiently replicates the compression and shear behavior of sand across a wide range of confining pressures and densities. A comprehensive parametric analysis has been conducted, encompassing a broad range of parameter variations. The principal objective is to present an innovative design approach concerning the bearing capacity of footings for diverse sand characteristics across an extensive array of sand properties. Additionally, a correlation has been established between the bearing capacity factors for strip and circular footings.

Keywords: Bearing Capacity; Strip Footing; Circular Footing; Sand; Finite Element; Hypoplastic Model.

1. Introduction

The bearing capacity of shallow footings on sandy soils is a well-documented topic in foundation engineering, having undergone substantial research in recent decades. Previous investigations mainly employed laboratory testing performed under one-gravity conditions [1–4]. Failure to follow similitude principles may result in an inaccurate representation of sand behavior [2, 5]. The application of these tests to evaluate analytical methodologies, including characteristic and limit state approaches, resulted in a misinterpretation of the behavior of sand under shallow footings. As stated by Bolton [3], sand bearing capacity solutions derived from large-scale field experiments proved inadequate to predict the actual field behavior. Employing bearing capacity values derived from laboratory experiments conducted under one-gravity conditions to predict prototype or field-scale footings would be considered inappropriate. Thereafter, the geotechnical centrifuge modeling technique was utilized to perform physical modeling in geotechnical engineering via experimental model tests, as demonstrated by numerous studies [4, 6–8]. It significantly improves our understanding of sand behavior under shallow footings. Many researchers have successfully developed empirical equations or design approaches to assess the bearing capacity of the soil. Centrifuge studies were utilized to validate analytical methods. When assessing the test findings, it is essential to examine additional variables to understand the behavior of the sand.

* Corresponding author: maramadan@kau.edu.sa; mohamedihr@mun.ca

http://dx.doi.org/10.28991/CEJ-2025-011-03-03

© 2025 by the authors. Licensee C.E.J, Tehran, Iran. This article is an open access article distributed under the terms and conditions of the Creative Commons Attribution (CC-BY) license (http://creativecommons.org/licenses/by/4.0/).

The bearing capacity classical solution defines the ultimate bearing capacity; q_u for a footing on sand surface can be calculated as:

$$q_u = \frac{1}{2}\gamma' B N_\gamma \tag{1}$$

where γ' is the effective unit weight of the sand, B is the footing width or diameter, and N_γ is the bearing capacity factor, which is dependent on sand unit weight. The classical solution suggests that N_γ can be calculated as a function of peak friction angle, ϕ_p. However, peak friction angle of sand ϕ_p is a function of mean effective stress p'. As can be seen in Figure 1, ϕ_p of sand decreases as the mean effective stress p' increases. Also, shown in (Figure 1) is that ϕ_p decreases as D_r decreases. Therefore, selecting an appropriate peak friction angle ϕ_p or mobilized friction angle ϕ_m is a challenge. The variability of N_γ based on the estimated approach has become a significant factor contributing to discrepancies among techniques for estimating q_u. The study by Diaz-Segura [9] reveals variations in maximum and minimum N_γ values derived from 60 different estimation methods, with equal ϕ_p ranging from 28º to 44º, showing differences of 246% to 267%.

The peak friction angle exhibited by the sand is determined by two distinct contributing factors [3]. The primary factor is related to the critical condition or the angle of constant volume friction ϕ_{cr}. The measurement of this angle is mostly dependent on the shape or structure of the sand particles. According to many researchers [2, 10–14], it is independent of stress level or sand density. The second component relates to the dilation of sand. The degree of dilation of the sand depends on the intensity, density, and shape of the sand [14]. Sand is a material influenced by both stress and density. The peak friction angle of the sand, ϕ_p, increases as the mean effective stress p' decreases and the relative density of the sand D_r increases. Extrapolating this phenomenon to the bearing capacity of shallow footings on sandy soils clarifies the non-linear characteristics of sand behavior under footing loads. The application of vertical loading causes continuous variations in both p' and D_r, leading to changes in the mobilized sand friction angle and, subsequently, the shear strength of the sand under the footing. As the load increases, some sections of the expected slip surface will reach the maximum friction angle and experience softening, while other sections will maintain a low strength level. Upon completion of the loading process, the shear strain levels reach a magnitude adequate to induce certain sections of sand along the slip surface to achieve the critical shear state before the limit load on the footing is attained. The phenomenon of concern is typically termed progressive failure, as several authors have noted [15–20]. Owing to the variability in the mean values of the principal stress and void ratios at various locations adjacent to the foundation, accurately determining the peak friction angle for the calculation of bearing capacity factors remains a considerable challenge [21].

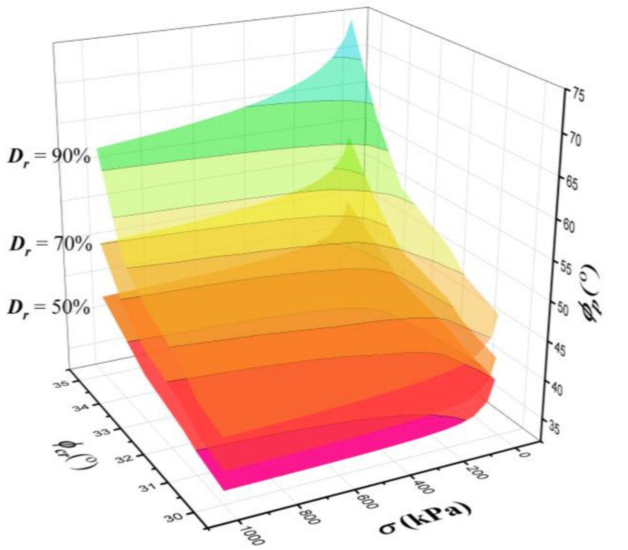

Figure 1. Variation of ϕ_p with p', ϕ_{cr} and D_r

Extensive research, encompassing both empirical and computational/analytical approaches, has been conducted on the phenomenon of the scale effect. Two separate factors affect the scale. The peak friction angle of the sand, ϕ_p, is contingent upon the value of p'. An increase in footing width is likely to have a larger zone of influence. An increase in the mean stress p' beneath the footing will lead to a decrease in the average ϕ_p. A footing of a smaller width will yield a diminished zone of influence. This indicates a reduction in the average mean stress ϕ_p and an increase in the mean ϕ_p. Footing width influences the bearing capacity in relation to the average stress and shear strength of the soil. The second part mainly relates to the small-scale testing that researchers usually perform to assess bearing capacity. The increase in bearing capacity was observed to occur at an accelerating rate when the ratio decreases, with d_{50} denoting the mean particle size of the sand. This phenomenon has been demonstrated in the works of De Beer [15]. It is typically called the particle size effect. The effect of particle size is not attributable to pressure. It is recommended that the ratio of footing width to particle size of the sand should not be less than 150, as per references [6, 15]. This effect is of considerable significance for physical model tests and may lead to unreliable conclusions. Therefore, caution should be taken when selecting experimental tests for the purpose of validating or comparing design approaches.

Although these analytical methodologies predominantly rely on a limit analysis solution, they exhibit variations in their assumptions concerning boundary conditions and the consideration of soil weight effects. Most of these methods simulate sand using a rigid-perfectly plastic stress-strain relationship. In particular, the calculation of the bearing capacity of shallow foundations is based on an associative flow rule assumption. The method of characteristics, adhering to rigid-perfectly plastic behavior and an associated flow rule, has been used by Zhu et al. [22] to examine the bearing capacity of circular and strip footings. The validation of the model was achieved through centrifuge tests, in which circular footings exhibited diameter ranges from less than 1 m to up to 10 m, and strip footings had widths extending up to 2.4 m. However, the investigation was confined to one type of sand with a relative density (D_r) of 90%. Within the analysis of characteristics, the angle of friction of the soil is integrated as a stress-dependent variable, and its value is adjusted based on the stress level during the computational procedures.

The results obtained from the characteristic methods were in good congruence with the calculated bearing capacity derived from both experimental tests and calculations employing an equivalent or mobilized friction angle corresponding to the mean normal stress along the failure surface. Both numerical analysis and experimental modeling show that the shape factor (s_γ) increases with footing dimension. The value of s_γ of the circular footings from the numerical analysis is up to 22% lower than the traditional value of $s_\gamma = 0.6$. They concluded that, according to their study conditions, using the traditional value of 0.6 is unconservative for small footings by up to about 25% but may be conservative for large foundations by about 5%. The studies by Chakraborty & Kumar [16] and Kumar & Khatri [17] integrate the variation of the angle of internal friction (ϕ) with respect to the mean principal stress (σ_m). An investigation was conducted using lower bound limit analysis in combination with finite elements and linear programming. An iterative procedure was introduced to address the dependence of ϕ on σ_m. Two well-established ϕ - σ_m curves of Toyoura and Hoston sands from the existing literature were utilized for circular and strip footings. It was concluded that the magnitude of N_γ significantly decreases as the width of the footing increases.

Furthermore, there exists a limited number of studies addressing the impact of the non-associative flow rule on bearing capacity. The Zero Extension Lines (ZEL) method had been implemented by Jahanandish et al. [18] and Veiskarami et al. [19] to calculate the bearing capacity factors both with and without accounting for the impact of stress on the friction angle of sand. For practical considerations, design charts were developed to examine the impact of foundation size on bearing capacity factor N_γ, utilizing Bolton's (1986) [3] equations for stress-level-dependent variations of soil friction angle. These design charts were restricted to a relative density (D_r) of 50% and critical state friction angles (ϕ_{cr}) of 30º, 35º, and 40º for circular footings. However, the charts were extended to a D_r of 75% for strip footing scenarios. The researchers indicated that the main goal of their study was to prevent overly conservative or potentially unsafe predictions that might result from assuming a uniformly distributed friction angle throughout the soil mass being analyzed.

An empirical method, derived from full-scale experimental and centrifuge tests of rigid foundations by Perkins & Madson [23], addresses the scale effects resulting from the nonlinear strength behavior and the impact of progressive failure on capacity using Bolton's equations. Consideration is also given to the shape of the footing. This method is advantageous as it simplifies the process of generating material property data. The analysis necessitates only an assessment of the relative density of the soil, the unit weight, and the constant volume friction angle. The design solution is iterative and can be easily programmed. An additional empirical method has been developed from Finite Element Modeling (FEM) of rigid rough footing on the sand surface, as proposed by Loukidis & Salgado [24]. The investigation employed a two-surface plasticity constitutive model following critical-state soil mechanics, which accommodates strain softening as well as both stress-induced and inherent anisotropy, in addition to non-associativity of the flow rule. Circular and strip footings of 1-3 m in diameter or width and 60% to 90% relative density were considered. Toyoura sand (ϕ_{cr} = 31.5º) and Ottawa sand (ϕ_{cr} = 30º) calibrated parameters were implemented in the model. Finite element (FE) simulations of strip footings indicate that the complete formation of the general shear mechanism manifests itself at large settlements.

In the context of dense sands, such settlements can significantly exceed those necessary to achieve the limit load (collapse), which spans a wide range from 5% to 30% of the footing width B, depending on the relative density and intrinsic properties of the sand. The bearing capacity factor N_γ exhibits a decreasing trend with an increase in the width of the footing and the unit weight of the sand. The FE results further suggest, and the experimental work by Janabi et al. [2] supported that the shape factor (s_γ) for circular footings, given a constant relative density, falls within the range of 0.7 to 0.9. Ultimately, the findings of the FE analysis can be instrumental in obtaining valuable correlations for N_γ, s_γ, and an equivalent friction angle to be used in the traditional bearing capacity equation. The results of the FE analysis are compared with experimental centrifuge tests using Toyoura sand (relative densities 58%-88%). Their design approach aligns with the general trend of the experimental tests, but they are about 20% lower on average and 50% at most.

The prior discussion indicates that several factors, such as particle morphology, footing width, mean effective stress, relative density, and progressive failure, affect the bearing capacity of a surface footing on sandy soil. The structural composition of the sand may be the principal factor influencing its behavior under load conditions. It is essential to understand that the composition of different types of sand shows considerable variances in their structural configuration. Many sand shear tests have shown that the behavior of sand shear strength can be affected by the starting fabric condition [4]. Sand shear strength is affected by the mean grain size d_{50} and the uniformity coefficient C_u, as demonstrated by the research carried out by Yamaguchi et al. [20] and Ueno et al. [25]. The dilation behavior of sand is expected to be influenced by its angularity. Therefore, it may be concluded that sands with the same peak friction angles demonstrate different behaviors. Discrepancies in mobilization friction angles and stress-strain behaviors are evident among sands with identical relative densities, D_r, and mean effective stresses, p'. Thus, the assessment of true bearing capacity may be inaccurate if the bearing capacity factors are calculated exclusively based on a constant ϕ_p.

In the literature, various methodologies have been proposed to predict the bearing capacity of both strip and circular footings. Early research focused on the variation of friction angles with stress [6, 20]. Subsequent studies expanded on these findings to incorporate the effect of footing size [4, 7, 16, 17, 22, 25, 26]. Other investigations focused on the dependency on stress and sand critical friction angle effects only [23, 27] or all aforementioned parameters [18, 24, 27] as part of design approaches. However, these studies have certain limitations regarding parameter boundaries. In recent years, due to the progressive advancements in the field of artificial intelligence, Machine Learning (ML) has been employed to predict the bearing capacity of sand utilizing existing databases [27–32]. However, the deployment of ML requires a sufficiently large dataset to avert the risk of overfitting the model. Given that the current experimental work database is insufficiently large for effective ML application, researchers resort to Finite Element Limit Analysis (FELA) to construct a database of the specified cases. This approach adheres to the methodologies of lower or upper limit analysis. It facilitates the creation of a model that can be compared with extant experimental work or partitioned into training and testing subsets to ascertain the model's validity. FELA offers the advantage of rapid convergence solutions, allowing for a large number of cases to be resolved expeditiously, which is a challenge presented by the finite element method (FEM) when employing sophisticated soil models. Although AI/ML technologies have demonstrated considerable success in geotechnical engineering, they remain in a state of development, and their practical implementation may necessitate further scholarly inquiry and validation [33].

Despite the extensive prior research on the bearing capacity of sandy soil, uncertainties and deficiencies persist regarding the utilization of the peak friction angle ϕ_p instead of the critical ϕ_{cr} or mobilized ϕ_m angles. Furthermore, the assumption of modeling the soil as a perfectly plastic material obeying associated flow in most analytical and numerical design approaches presents additional challenges. This model is the most commonly used for representing soil behavior; however, it exhibits certain limitations compared to advanced models. Significant shortcomings include its inability to precisely capture soil strength as described by critical state soil mechanics, its inability to represent nonlinear stress-strain behavior, and its deficiency in accounting for the evolution of soil fabric anisotropy under applied loading [34].

The present study utilizes a three-dimensional finite element model (3D-FEM) to simulate strip and circular footings on a dry sand surface. The hypoplastic sand model is adopted to address the implications of stress-density behavior in sand. It has the benefit of extensive availability for implementation in commercial finite element software. The values of the soil parameters are accessible for a wide range of soil types, and calibration routines are provided to facilitate the calibration process of the parameters. From a soil mechanics perspective, the hypoplastic model is also capable of accounting for effects related to changes in the void ratio. In contrast to ideal elastoplastic models governed by the Mohr–Coulomb and Drucker–Prager failure criteria, it skillfully emulates the nonlinear behavior of soils. Moreover, the incorporation of the critical state concept allows the model to proficiently represent the progression of failure surfaces, thereby facilitating the precise modeling of strain hardening or strain softening phenomena in sand under diverse initial conditions [35]. Different calibrated sands have been implemented in the study. A parametric investigation is also performed. The primary objective of this research is to evaluate the anticipated bearing capacity factor across different sand characteristics and to propose a solution applicable in a broad spectrum of sand characteristics. Additionally, rather than providing a direct shape factor, a relationship between the bearing capacity factors of strip and circular footings has been derived from the findings. The current investigation is part of a broader research project aimed at examining the ring footing under combined loading conditions. Both the strip and circular footing behavior should be explored under identical three-dimensional conditions.

2. Problem Definition

A Finite Element Model (FEM) was developed in PLAXIS 3D for the current work. The software accommodates many constitutive soil models and enables users to incorporate their own material subroutines. The current study can be divided into six phases. The first phase is the establishment of FEM. FEM should go for validation in both mesh size and boundary condition effects. In addition, a careful selection of input parameters for the soil model has been made. The following phases include parameter selection, parameter sensitivity analysis, and analysis of the results. Finally, design approaches have been recommended and compared with available centrifuge tests and other design approaches in the literature. The summaries of the flow charts for the current study phases are shown in Figure 2. The following details pertain to model geometry, meshing, and constitutive models.

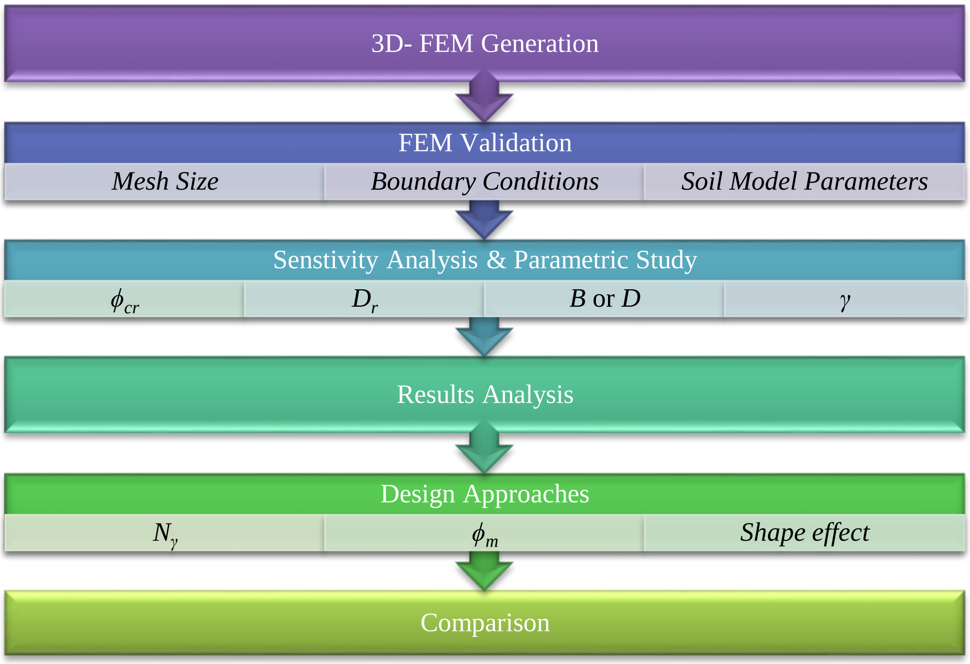

Figure 2. Flow Chart of the research methodology

2.1. Model Geometry and Meshing

Three-dimensional modeling has been used to ensure consistent application of the same element type and constitutive material models in subsequent studies for ring footing scenarios, as seen in Figure 3. The simulation uses an unstructured mesh of ten node tetrahedral volume elements. It provides a second-order interpolation of displacements. Four-point Gaussian integration has been used within the volume element. Due to the centric vertical loading's symmetry, only one-quarter of the circular footing model and one-half of the strip footing model are simulated. To satisfy the plane strain conditions in the strip footing model, the footing length is identical to the length of the model in the y-direction. The model length in the y-direction is constrained to 1 meter to minimize computational costs. Various lengths have been analyzed using the same proportionate mesh size. The outcomes of all instances were consistent. According to the study results of Woodward et al. [36], the selection of boundary conditions was made while ensuring an adequate distance from the edge of the footing. The dimensions of the model base and vertical sides are approximately 7 and 10 times the diameter of the footing far from the footing edge, respectively, in Figures 3-a and 3-b. While for the strip footing case, the dimensions of the model base and vertical sides are approximately 10 and 15 times the width of the footing far from the footing edge, respectively.

The vertical sides are subject to constraints that limit their horizontal displacement but allow for unrestricted vertical displacement. The model base is restricted to all displacements in any direction. The model mesh is configured to provide a finer mesh near areas of high stress and deformation across the foundation. The mesh refinement in the designated area is three times the width of the footing, exceeding the refinement level of the remainder of the model. Zone dimensions were established by analyzing multiple models with varying footing widths to ensure that the failure surface remained confined within this specified area. The models have undergone control measures to ensure that the mesh meets the requirement of a minimum size le of 0.05 of the footing width [36]. A sensitivity study was performed to evaluate the influence of the mesh size and the size of the model on the results. Figure 4 illustrates the error in the maximum bearing capacity as it relates to the minimum mesh size. An error of less than 0.1% was found in le / B.

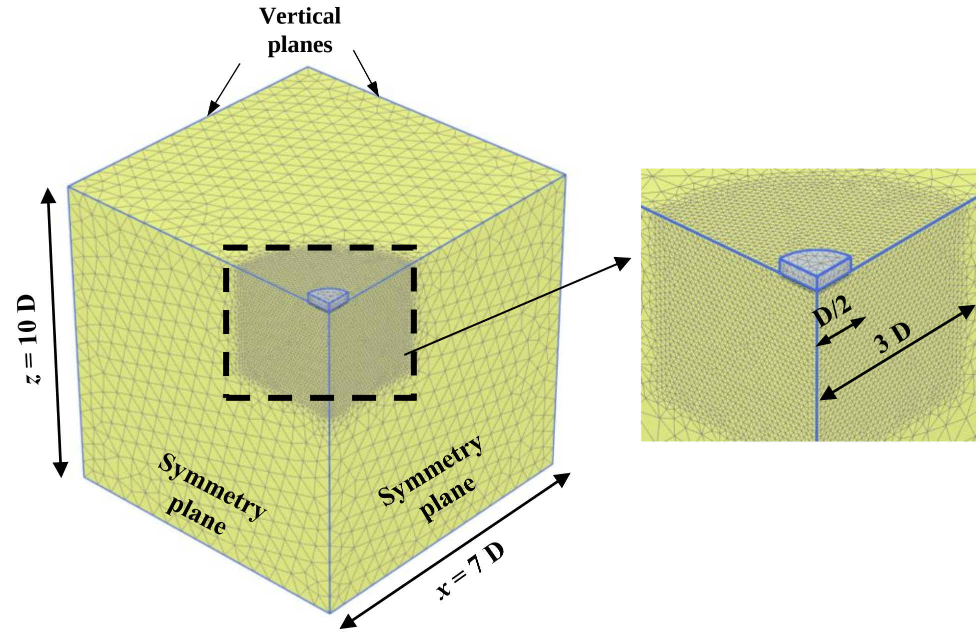

(a) Circular footing model

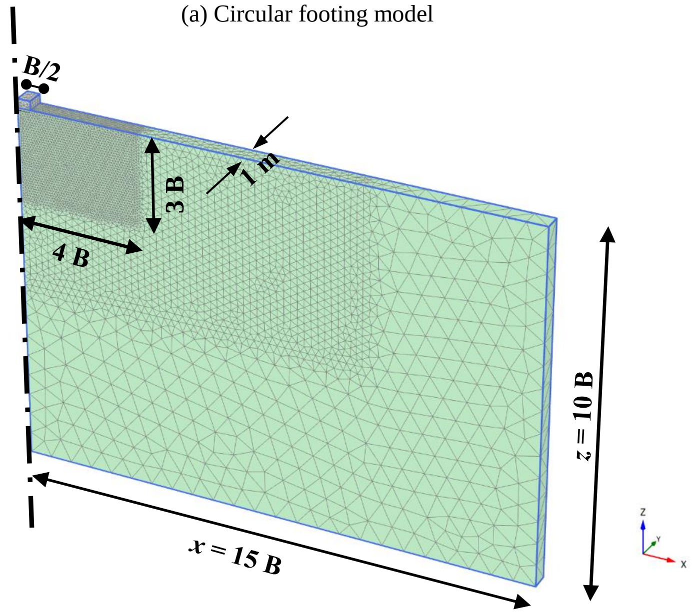

(b) Strip footing model

Figure 3. FEM geometry and meshing

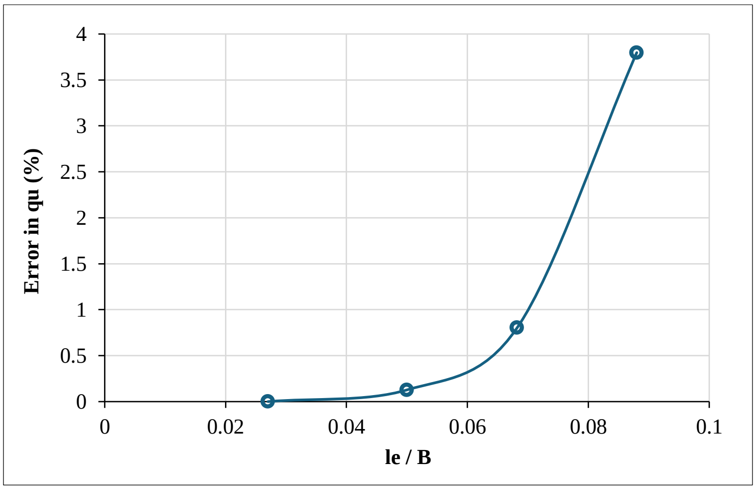

Figure 4. Geometry and meshing optimization

The footing simulation involves analyzing a rigid body subjected to a predetermined vertical displacement. The rotation of all axes and the horizontal displacement are constrained. In this investigation, an interface element is used to simulate the rough soil-footing interface. Mohr friction criteria are utilized to model the interaction. The interface friction angle ϕ_{int} associated with the contact was indicated to have a value of 28º, which is equivalent to a friction coefficient of about 0.5, as stated in Ramadan & Meguid [37]. No tension was allowed for the interface parts.

2.2. Hypoplastic Sand Constitutive Model

Hypoplasticity represents an advanced constitutive modeling approach, distinguished from the conventional elastoplasticity methodology. It provides a framework for property-based asymptotic constitutive modeling of soils. Within this theoretical context, constitutive relations can be derived from the intrinsic properties of granular materials. The constitutive relation employs a distinctive tensorial equation to delineate the progression of stress in relation to deformation. The model integrates established principles from soil mechanics, including critical states, barotropy (the correlation between stiffness and strength with stress level), pyknotropy (the correlation between stiffness and strength with density), and a stress-dilatancy relationship. The hypoplastic constitutive model is heavily based on the concept of a critical state. Although its mathematical structure is relatively simple, numerous complex phenomena associated with barotropy and pyknotropy have been extensively examined. The hypoplastic model is a potent technique to simulate soil behavior in various engineering applications. Furthermore, the stress-dilatancy relationship facilitates accurate prediction of soil deformation and failure under various loading conditions. To achieve this objective, it is imperative that the constitutive model be contingent upon the void ratio. The initial version of the hypoplastic model developed for sands only integrated the stress state as a state variable, leading to its insufficiency in accurately representing soil behavior. As a result, subsequent laws concerning hypoplasticity were devised with the objective of incorporating the effects of barotropy and pycnotropy in the soil. To achieve these goals, we integrated a novel state variable into the rate tensorial equation, specifically, the void ratio.

2.2.1. Model Formulation

In the hypoplastic sand model, the concept of critical state is defined by integrating a distinctive relationship between the mean stress p' and the limiting void ratios at its minimum density. e_i, at the critical state e_c, and at the maximum density e_d as

$$\frac{e_i}{e_{io}} = \frac{e_c}{e_{co}} = \frac{e_d}{e_{do}} = \exp\left[-\left(\frac{3p}{h_s}\right)^n\right] \tag{2}$$

where h_s and n are constitutive parameters as described in Table 1.

Table 1. Hypoplastic Sand Model Parameters

Parameter	Description	Calibration Method
ϕ_{cr} (°)	Critical friction angle	Angle of repose or drained triaxial test
h_s (MPa)	Granular hardness	Oedometer test at e_{max}
n	Controlling the curvature of the compression line	
e_{do}	Void ratio at the lowest density at p′=0 kPa	Cyclic shearing or standard e_{min} test
e_{co}	Void ratio at the critical state line at p′=0 kPa	Standard e_{max} test
e_{io}	Void ratio at the highest density at p′=0 kPa	1.15 – 1.2 e_{max}
α	Controlling the peak friction angle	Drained triaxial test
β	Controlling the bulk and shear stiffness	

The tensorial equation was revised to integrate barotropy and pyknotropy, each characterized by its respective scalar functions. f_s and f_d, respectively, according to

$$\dot{T} = f_s(\mathcal{L}{:}\mathbf{D} + f_d \mathbf{N}\,\|\mathbf{D}\|) \tag{3}$$

where $\mathcal{L}$ is a fourth-order constitutive tensor, **N** is a second-order constitutive tensor, and **D** is a stretching tensor. The scalar factors f_s and f_d are employed to integrate the influence of the average pressure and density, respectively. These factors are also designated as barotropy and pyknotropy factors. The stiffness of the soil is governed by the factor f_s. The calculation can be deduced from variables f_b and f_e.

$$f_s = f_b \cdot f_e \tag{3.1}$$

$$f_b = \frac{h_s}{n}\left(\frac{1+e_i}{e_i}\right)\left(\frac{e_{i0}}{e_{c0}}\right)^{\beta}\left(-\frac{tr\boldsymbol{T}}{h_s}\right)^{1-n}\left[3 + a^2 - a\sqrt{3}\left(\frac{e_{i0}-e_{d0}}{e_{c0}-e_{d0}}\right)^{\alpha}\right]^{-1} \tag{3.2}$$

where;

$$a = \frac{\sqrt{3}(3-\sin\phi_{cr})}{2\sqrt{2}\sin\phi_{cr}} \tag{3.3}$$

$$f_e = \left(\frac{e_c}{e}\right)^{\beta} \tag{3.4}$$

f_e increases the stiffness as void ratio decreases. This increase is controlled by parameter β.

$$f_d = \left(\frac{e-e_d}{e_c-e_d}\right)^{\alpha} = r_e^{\alpha} \tag{3.5}$$

where α is a parameter that controls peak friction angle and r_e is the relative void ratio.

Figure 5 shows the simulation of a single element triaxial test performed on Toyoura sand across a range of densities, corresponding to various initial void ratios. The hypoplastic constitutive model proficiently captures the hardening and softening behaviors of sand. With a decrease in relative density, there is a concomitant decrease in the sand dilation. Alterations in the void ratio arise in response to fluctuations in stress and density.

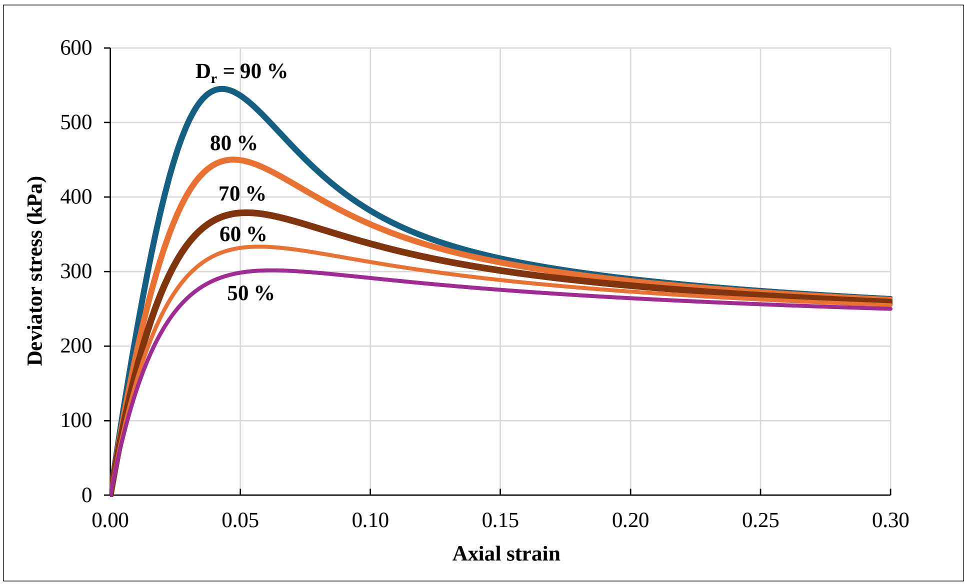

Figure 5. Stress-strain curves under triaxial testing conditions at different D_r (Toyoura sand – confining stress = 100 kPa)

2.2.2. Model parameters Validation

The existing literature encompasses a substantial number of well-calibrated models for hypoplastic sand. Sands with a wide spectrum of critical friction angles (ϕ_{cr}) and mean grain size (d_{50}) were selected for the present study. Tables 2 and 3 display the parameters for the hypoplastic sand model alongside the physical characteristics of the selected sands, respectively. The hypoplastic sand model has been integrated into Plaxis 3D software as a user-defined material [38].

Table 2. Model Parameters Values for Different Sands

Sand Name	ϕ_{cr} (°)	h_s (MPa)	n	e_{do}	e_{co}	e_{io}	α	β	*Reference*
Komorany	35	50	0.2	0.35	0.87	1.04	0.26	4	Mašín & Duque [39]
UWA silica	34	1354	0.366	0.49	0.79	0.86	0.18	1.27	Qiu & Grabe [40] and Qiu & Henke [41]
fine Karlsruhe	33.1	4000	0.27	0.677	1.054	1.212	0.14	2.5	Wichtmann & Triantafyllidis [42]
Toyoura	31.5	2600	0.27	0.61	0.98	1.1	0.14	3	Mašín [43] and Ng et al. [44]
Ottawa 50-70	30	4900	0.29	0.49	0.76	0.88	0.12	1	Wegener & Herle [45]

Table 3. Sands Physical Properties

Sand Name	d_{50} (mm)	C_u	G_s	e_{min}	e_{max}	*Angularity*	*Reference*
Komorany	1.183	3.99	2.65	0.35	0.87	rounded	Mašín [43]
UWA silica	0.49	1.38	2.67	0.49	0.79	rounded	Qiu & Henke [41] and Chow et al. [46]
Fine Karlsruhe	0.14	1.5	2.65	0.677	1.054	sub-angular	Wichtmann & Triantafyllidis [42]
Toyoura	0.16	1.46	2.64	0.61	0.98	sub-angular	Mašín [43] and Ng et al. [44]
Ottawa 50-70	0.34	2.3	2.65	0.49	0.75	rounded to sub-rounded	Wegener and Herle [45]

The selected sands have been adequately calibrated using a standardized method [47]. The calibration methodology has been extensively elaborated upon by numerous scholars [43, 47, 48]. The calibration procedures utilized across all the referenced sources were uniform. Furthermore, physical models were used to support certain of these models.

Automatic calibration tools are used to adjust the hypoplastic sand model through soil element tests. Komorany sand calibration is carried out using Excalibre, an online calibration tool developed by Gudehus et al. [38], accessible at (*https://soilmodels.com/excalibre/*). This method involves using a sensitivity analysis similar to the stochastic calibration technique. During calibration, emphasis is mainly on the objective error function, with less focus on the physical relevance of the model parameters. Setting parameter limits is essential to maintain physical relevance, as highlighted in Mašín & Duque [39].

Calibration of UWA silica sand was achieved through the application of centrifuge modeling, spudcan penetration, and pile driving simulations [40, 41]. Fine Karlsruhe sand was subjected to a series of oedometer and triaxial compression tests in research carried out by Wichtmann and Triantafyllidis [42]. A hypoplastic sand model was fine-tuned using an extensive database encompassing various relative densities. The calibration process for Ottawa 50-70 sand was documented in Wegener & Herle [45].

Extensive research has been conducted on Toyoura sand, which has been used for the calibration of hypoplastic sand models. Many studies have documented the calibration of Toyoura sand [43-45, 48-50]. The present investigation employs finite element method (FEM) simulations of circular and strip footings on a dense Toyoura sand surface as previously conducted in centrifuge testing by Okamura et al. [7] to determine suitable model parameters. A comprehensive investigation was conducted on the spectrum of values related to the parameters of the hypoplastic model. The validation of the model parameters proposed by Ng et al. [44] was carried out by means of a centrifuge test involving footing diameters / widths of 2 m and 3 m, which produced analogous results, as shown in Figure 6. To ensure alignment with the experimental data, it became necessary to adjust the critical friction angle ϕ_{cr} to 31.5˚. This little alteration has been suggested by previous research efforts [12, 24, 51] as well. Furthermore, it is pertinent to note that the design methodology advanced in this investigation will be subject to a comparative assessment with physical model experiments, as well as established numerical models documented in the existing literature. The current study will conduct an analysis of a centrally loaded vertical footing on a sand surface.

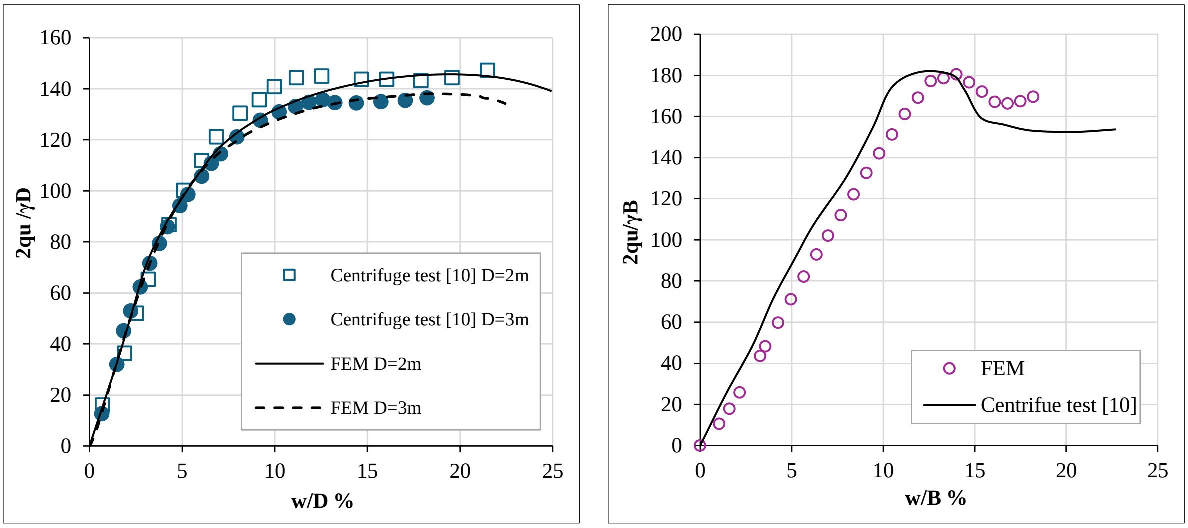

(a) (b)

Figure 6. Normalized load – displacement comparison with centrifuge tests (a) circular footing, (b) strip footing (*B* = 2 m)

2.3. Ultimate Bearing Capacity qu Selection

The ultimate soil bearing capacity is defined as the maximum average pressure that a foundation can impose on the soil without causing shear failure. The attainment of the bearing capacity is marked by reaching a state of constant stress. In the cases of strip footing, the bearing capacity is determined at the maximum load. In contrast, for circular footing scenarios, foundation load tests often do not achieve the maximum stress level due to the rearrangement of soil particles beneath the foundation during progressive failure or due to the limitations of field or experimental equipment. Bearing capacity can be identified at the intersection point of the two linear segments on the load-displacement graph, whether observed on a standard or logarithmic axis [51, 52]. The use of the method in this research is corroborated by evidence from numerous centrifuge and field experiments [7, 22, 53–57]. All results are presented in terms of the bearing capacity factor $N_{\gamma\text{-}strip}$ or $N_{\gamma\text{-}circle}$ without considering the shape factor effect for the circular footing.

3. Sensitivity Analysis

Sensitivity analysis is a methodological approach used to determine the significance of the input variables considered and their respective effects on the output variable. The objective is to discern the manner in which each variable affects the outcome of the result. This research conducted an independent variable importance analysis to assess the impact of four input parameters, specifically γ, D or B, ϕ_{cr}, and D_r, on the output N_γ.

The linear regression model assumes a linear relationship between the input parameters and the output. The regression coefficients ($\beta_1, \beta_2, \ldots, \beta_D$) are estimated using the least squares method, which minimizes the sum of squared residuals. The sensitivity indices are computed by normalizing the absolute values of the regression coefficients.

$$S_i = \frac{|\beta_i|}{\sum_{j=1}^{D} |\beta_j|} \tag{4}$$

where Si is the sensitivity index for the i-th parameter. βi is the regression coefficient for the i-th parameter.

Figure 7 illustrates a column plot that clarifies the significance of each input parameter in relation to the output parameter. The analysis reveals that the critical state friction angle (ϕ_{cr}) exerts the most substantial influence on the bearing capacity factor (N_γ) for both strip and circular footings. Subsequently, the unit weight of the soil (γ) acts as the second level of importance in the case of strip footings, followed by relative density (D_r) and width of the footing (B). However, in the case of circular footings, the footing diameter emerges as the second most important factor, followed by relative density (D_r) and the unit weight of soil (γ). Despite the variation in the importance of the parameters, they all play a significant role in determining the bearing capacity of either the strip or circular footing on the sand surface. The interaction among all parameters will be explained after the results are presented and discussed.

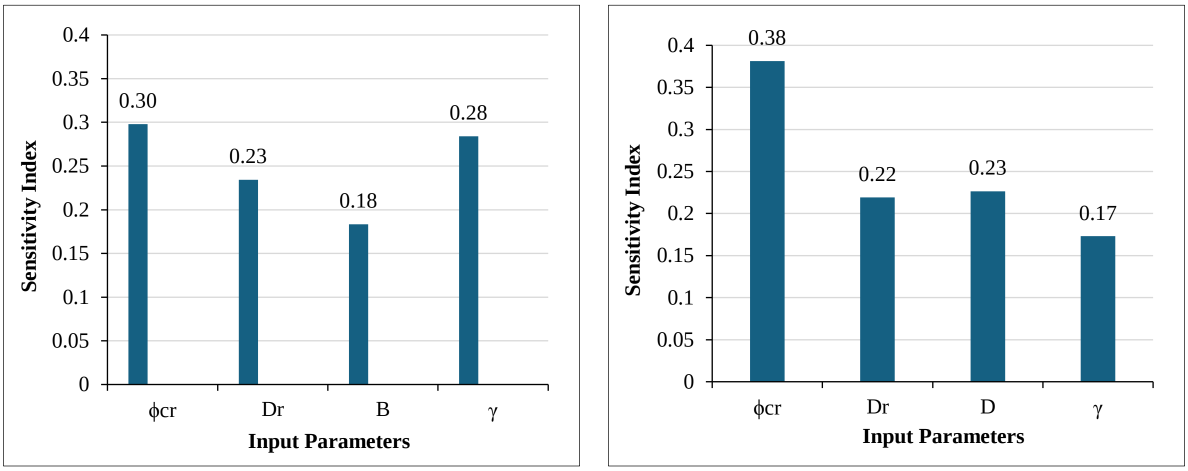

(a) (b)

Figure 7. Sensitivity analysis of input parameters (a) strip footing, (b) circular footing

4. Parametric Study Results and Discussion

The finite element method (FEM) was utilized to perform a comprehensive set of parametric investigations, comprising about 257 simulations (132 for circular footing and 125 for strip footing). In conjunction with the critical friction angle ϕ_{cr}, which constitutes the principal parameter in this investigation, it is imperative to incorporate additional parameters when assessing the load-bearing capacity of a circular foundation located on a sand surface subject to a vertically centered load. These parameters exert a profound influence on the behavior of the sand. The study evaluates the widths or diameters of the footings (B or D). For strip footing scenarios, footings with dimensions of 1.5, 2, 3.5, 7, and 10 meters were examined. In contrast, for circular footing scenarios, diameters of 1.5, 2, 3, 4.36, 7, and 10 meters were analyzed. The selected sizes of the footings have been determined through centrifuge experiments carried out by [7, 55, 56]. The relative density of the sand (D_r) has emerged as a crucial determinant in the regulation of the vertical bearing capacity of circular footings on the sand. This study includes relative densities of sand at intervals of 50%, 60%, 70%, 80%, and 90%. The variation in relative densities of sand provides a unique resolution for the bearing capacity of sand characterized by medium to high density.

4.1. Critical Friction Angle of Sand ϕ_{cr}

As discussed before, the critical state friction angle of the sand is a contribution of many factors, including particle size and shape or structure. The increase in either particle size or particle angularity increases ϕ_{cr}, Tables 2 and 3. Comparing Ottawa sand and Komorany sand, both are rounded. However, the larger particle size of Komorany sand causes an increase in ϕ_{cr}. Comparing Ottawa sand of rounded particles with Toyoura sand and fine Karlesruhe sand of angular particles, ϕ_{cr} increases due to angularity. Both particle size and shape will increase the interlocking between particles and consequently increase the bearing capacity. The correlation between the bearing capacity factor (N_γ) and the critical friction angle (ϕ_{cr}) can be discerned through the analysis of the load displacement curves of the sands with different values of ϕ_{cr}, which range between 30˚ and 35˚ (Figure 8-a). The ultimate bearing capacity of the sand, q_u, decreases with a reduction in the critical friction angle, ϕ_{cr}, while maintaining constant conditions for relative density, D_r, and footing diameter, D. A similar pattern is evident for strip footing cases, as illustrated in Figure 8-b. It is evident that progressive failure is manifested in strip footing cases, yet it is scarcely discernible in circular footing instances with a critical friction angle (ϕ_{cr}) of 35º. In strip footing cases, general shear failure is observed at high values of ϕ_{cr}, converting to local shear failure as ϕ_{cr} diminishes. At a lower ϕ_{cr} of 30º, the presence of local shear failure is noted. The confinement of soil beneath the strip footings is comparatively less effective than that under the circular footings. This decreased confinement facilitates the propagation of shear failure along the entire length of the footing, resulting in progressive failure. In sandy soils, the behavior of strip footings is predominantly governed by plane strain conditions, which promote the distinct formation of progressively developing shear zones. Conversely, the behavior of circular footings is governed by axisymmetric conditions, enhancing soil stability and inhibiting the progressive formation of shear zones. Figure 9 shows the distribution of the void ratio for the circular footing cases. It supports the results observed from the load displacement curves. In all cases, a wedge zone characterized by high sand density is formed below the footing. However, as the load increases, the boundary of the wedge zone is restricted, and shear bands are generated obeying the failure criterion. The void ratio distribution illustrates an increase in void ratio at the wedge boundary, where shear bands emerge. With an increase in ϕ_{cr}, sand exhibits the same local shear failure but with a stiffer response. On the contrary, at a higher ϕ_{cr} of 35˚, general shear failure is little evident at large strain, characterized by a void ratio that achieves a limit or critical state corresponding to the critical friction angle of the sand along the slip surface of the shear failure. Similar behavior is observed in cases of strip footing. General shear failure arises at a high ϕ_{cr} of 35˚ (Figure 10-a), while local shear failure is apparent at lower values of ϕ_{cr} (Figure 10-c).

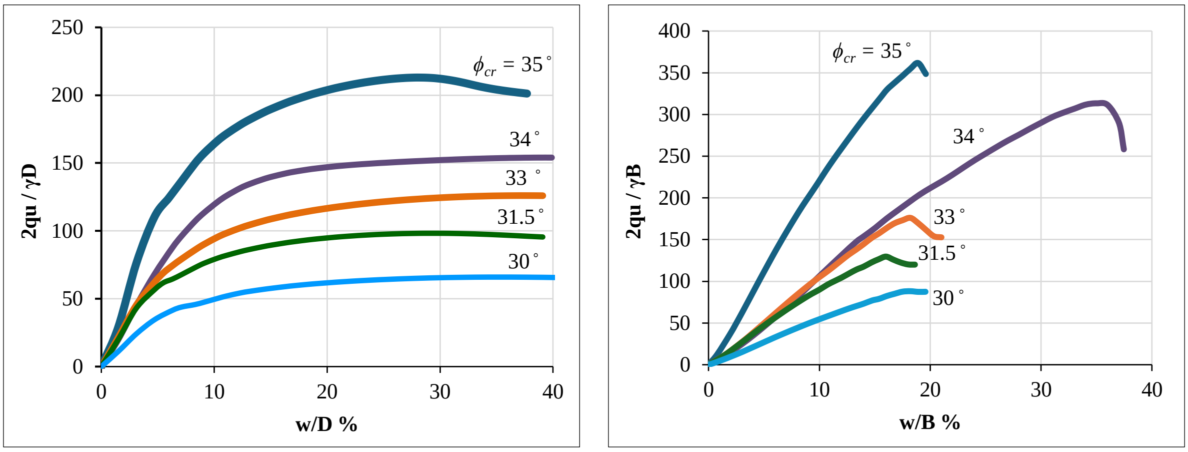

(a) (b)

Figure 8. Normalized ultimate bearing capacity – displacement curves for different sands at *Dr* = 70%: (a) *D* = 2 m, *circular Footing*, (b) *B* = 2 m, *Strip Footing*

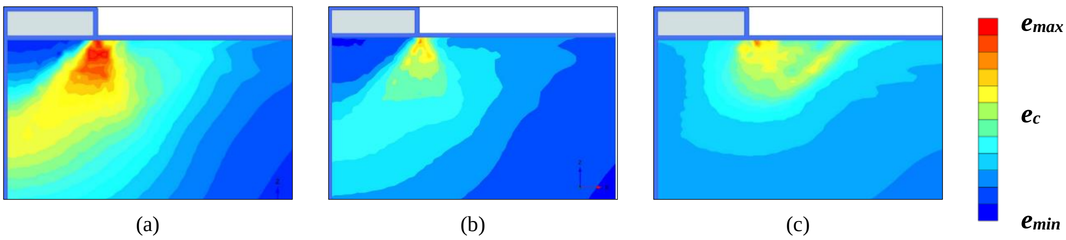

(a) (b) (c)

Figure 9. Distribution of void ratio at different ϕ_{cr} (a) 30˚, (b) 33˚, and (c) 35˚

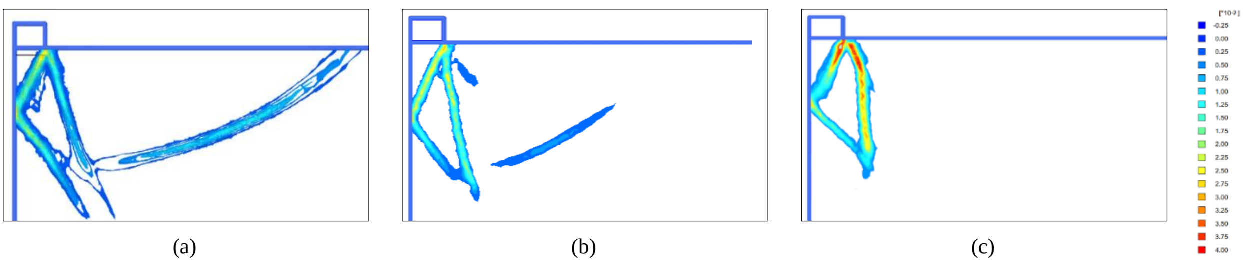

(a) (b) (c)

Figure 10. Incremental shear strain at the end of loading for *B* = 1.5 m (a) ϕ_{cr} =35º, D_r =80%, (b) ϕ_{cr} =35º, D_r =60%, and (c) ϕ_{cr} =31.5º, D_r =80%

4.2. Sand Relative Density D_r

Various studies have examined the relationship between relative density (D_r) and the ultimate bearing capacity of sand (q_u), consistently underscoring the crucial significance of D_r. When evaluating the effect of D_r, caution must be exercised with respect to the experimental investigations documented in the literature. One-gravity (low stress) tests conducted under loose sand conditions may exhibit progressive failure similar to dense sand at the prototype scale under identical loading conditions [58]. However, in prototype scale and at the same stress level, dense sand (D_r = 90%) has a smaller void ratio than medium sand (D_r = 50%). This means that to reach failure corresponding to critical state conditions, dense sand is far from the critical void ratio than medium sand of less D_r. So, the chance of progressive failure occurrence is much in denser sand than looser sand at the prototype scale (moderate stress level). Figures 10-a and 10-b corroborate this finding, showing that the incremental shear strain at residual strength decreases significantly as D_r reduces from 80% to 60% in strip footing cases. As the relative density of the sand (D_r) increases, the interlocking between the sand particles is enhanced, thereby increasing the bearing capacity of the sand. This effect is clearly demonstrated in Figures 11-a and 11-b for circular and strip footing scenarios. In cases of circular footing, no progressive failure or general shear failure is observed. Conversely, in strip footing scenarios, there is a significant occurrence of progressive failure. However, as D_r decreases, progressive failure diminishes, transitioning the failure mode from general to local shear failure.

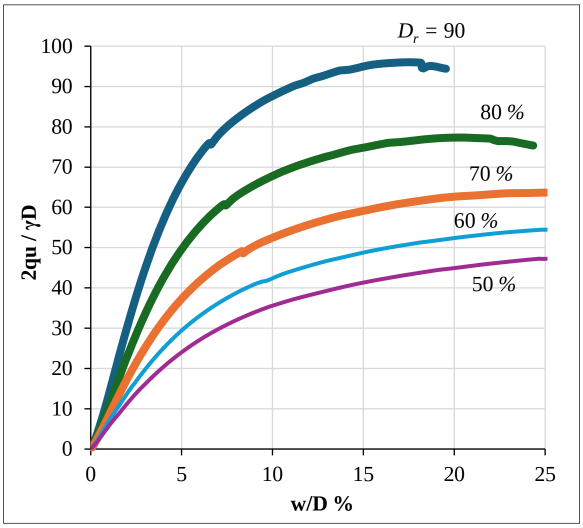

(a)

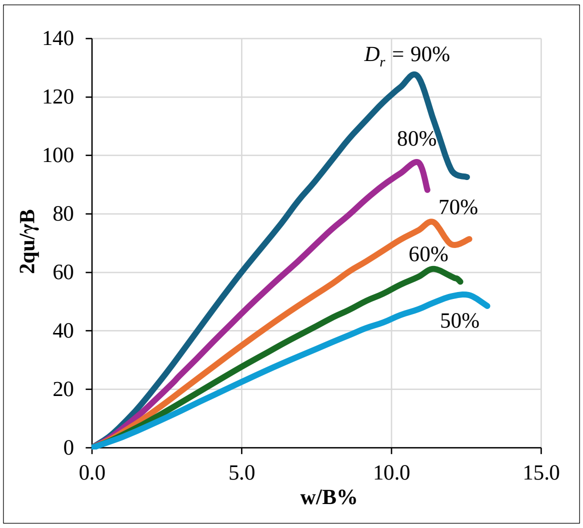

(b)

Figure 11. Normalized ultimate bearing capacity – settlement curves for Toyoura sand at different D_r (a) circular footing D = 3 m, (b) strip footing B = 3.5 m

4.3. Footing Size

The size of the footing has the same significant effect as the relative density of the sand D_r. It is related to the stress level under the footing. The anticipated bearing capacity factor for footings with smaller diameters is higher compared to that of larger diameter footings, attributable to the increased shear strength at diminished confining stresses or shallower depths. Progressive failure is more pronounced under circumstances of reduced confinement or when using smaller footing diameters. The bearing capacity factor N_γ is generally higher for smaller footing sizes., as demonstrated in Figure 12. General shear failure is observable for strip footings with a diameter of $B \leq 3.5$ m, coincident with the void ratio reaching a critical threshold along the shear slip surface. However, an increase in the foundation size to 7 meters or 10 meters results in the occurrence of local shear failure. Although both scenarios exhibit gradual failure during the mobilization of bearing capacity, the presence of a slip surface is less perceptible in instances with larger footing diameters. In cases involving circular footings, neither progressive failure nor general shear failure is observable as the relative density (D_r) and the critical state friction angle (ϕ_{cr}) decrease. A minor instance of general shear failure manifests at a diameter (D) less than 3 m, corresponding to a ϕ_{cr} of 35º and dense sand conditions. The influence of footing size diminishes for larger footings (7 m and 10 m) at reduced ϕ_{cr} values and decreasing D_r, applicable to both circular and strip footings, as depicted in Figure 12. The results by Zhu [56] from centrifuge tests conducted on dense sand with a relative density (Dr) of 90% and footing diameters ranging between 0.5 and 10 meters corroborate the present results. Their circular footing centrifuge tests did not exhibit any signs of progressive failure. However, the silica sand utilized in their experiments possesses a critical state friction angle (ϕ_{cr}) approximately between 32º and 33º, indicating that the potential for progressive failure occurrence is absent.

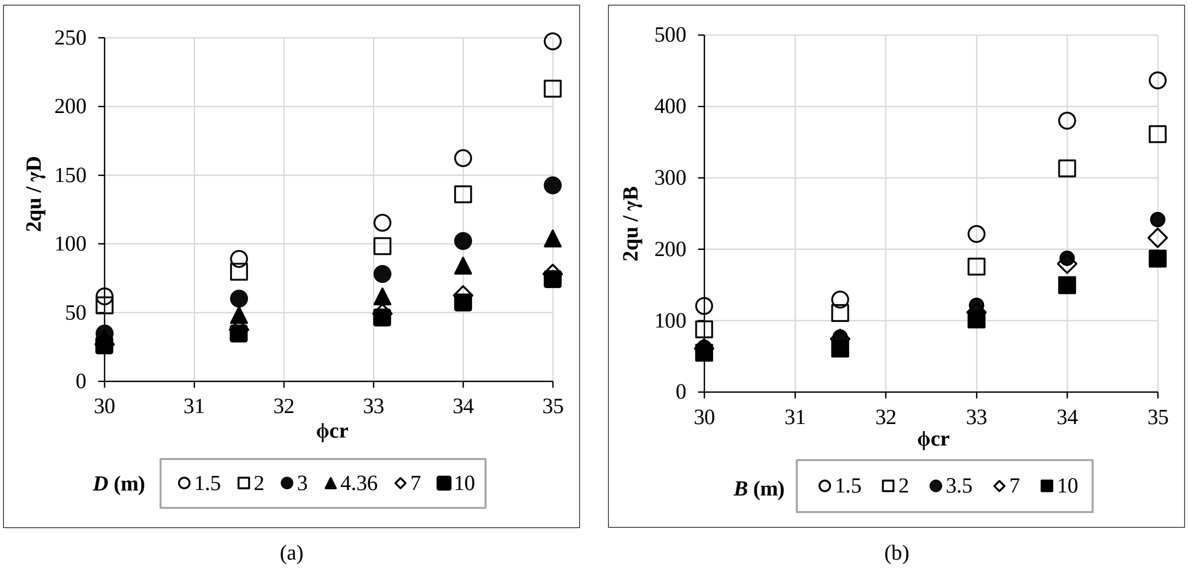

Figure 12. Normalized ultimate bearing capacity versus ϕ_{cr} for different footing diameters (D_r = 70%) (a) circular footing, (b) strip footing

4.4. Settlement – Footing Width or Diameter Ratio *w/B*% or *w/D*%

The findings of this investigation indicate that the settlement needed to reach the ultimate bearing capacity lies within the interval of *w/D* % = 8 - 12% for the circular footing. Except for UWA, the ultimate bearing capacity for all strip footing cases lies within the range of *w/B* % = 10 - 20%. For strip footing cases, the results for silica sand (UWA) indicate that it achieves peak values at a *w/B* ratio of up to 35%. UWA sand has an initial stiffness close to fine karlesruhe sand. This means that its stiffness is softer than expected. This soft behavior could not be observed clearly in circular footing cases due to the confinement under circular footing as discussed before. However, as such confinement releases, the soft stiffness appears clearly in strip footing cases. This less stiffness will not affect the ultimate bearing capacity, but it will cause to be mobilized at larger strain. Comparable behavior was observed by Zhu et al. [22] at *w/B* = 25% for silica sand at a relative density of 90% and a footing width of 2.4 m. The observations reported in this study align with findings from the existing centrifuge test literature. In general, for all cases, it is noted that lower values of settlement-footing size ratio are correspond to higher relative density, smaller footing size and higher critical friction angle ϕ_{cr}. On the contrary, as both the relative density D_r and the critical friction angle ϕ_{cr} decrease, the ultimate bearing capacity is attained with greater settlement. The range of observations recorded in this study aligns with earlier findings in the research literature on centrifuge tests. Centrifuge tests conducted by [7, 8, 59] indicate peak values at an average *w/B* of 15%. The initial slopes of the curves and the ultimate bearing capacity show a favorable correlation with the empirical results within the spectrum of the critical friction angle ϕ_{cr} for the sand. For circular footings, a range of 7-9% was observed by Kutter et al. [60] at a relative density (D_r) of 94%, while a value of approximately 10% at D_r of 80% was documented by Jensen and Lehane [61]. The load-displacement curves observed in this study are similar to the results from centrifuge tests conducted by Zhu [56] on silica sand with a relative density (D_r) of about 90%. Furthermore, the load-displacement curves for Toyoura sand which exhibits a D_r of approximately 90% [7] also reveal similar tendencies (Figure 6-a).

5. Proposed Design Approaches

Through the re-evaluation of the results of the present study, the incorporation of a stress level parameter ($\gamma D/p_a$ or $\gamma B/p_a$) [4, 7, 26, 55, 62] into the analysis becomes now feasible. The term p_a denotes the atmospheric pressure; approximately equal to 100 kPa; and is used to account for the influence of both the density of sand and the size of the footing. Presentation of results with respect to this metric facilitates a more exhaustive analysis. All the results of the current study are graphically represented in Figure 13 as a three-dimensional plot of the relative densities of the sand D_r, the stress level parameter $\gamma D/p_a$ or $\gamma B/p_a$, and the bearing capacity factor N_γ at different levels of ϕ_{cr}. The variation in the bearing capacity factor, $N_{\gamma\text{-}circle}$, is shown in Figure 13-a as a function of $\gamma D/p_a$ or $\gamma B/p_a$. The observable influence of the critical friction angle of the sand, ϕ_{cr}, is clear. Reducing ϕ_{cr} from 35° to 30° results in a substantial reduction in the value of $N_{\gamma\text{-}circle}$ within the $\gamma D/p_a$ or $\gamma B/p_a$ range of 0.2 to 2.0. As the critical angle ϕ_{cr} decreases, there is a corresponding reduction in the decrease rate. Moreover, it can be shown that the relative density of sand exerts a significant impact. A perceptible reduction in the value of $N_{\gamma\text{-}circle}$, specifically from 700 at $\gamma D/p_a$ = 0.25 to approximately 40 at $\gamma D/p_a$ values exceeding 1.7, can be observed when D_r is 90%. In the case of a lower relative density of sand (D_r = 50%), the differences observed within the specified range exhibit a comparatively smaller magnitude, ranging from 100 to 20. The same trend can be observed for cases of strip footing with higher values of $N_{\gamma\text{-}strip}$ (Figure 13-b).

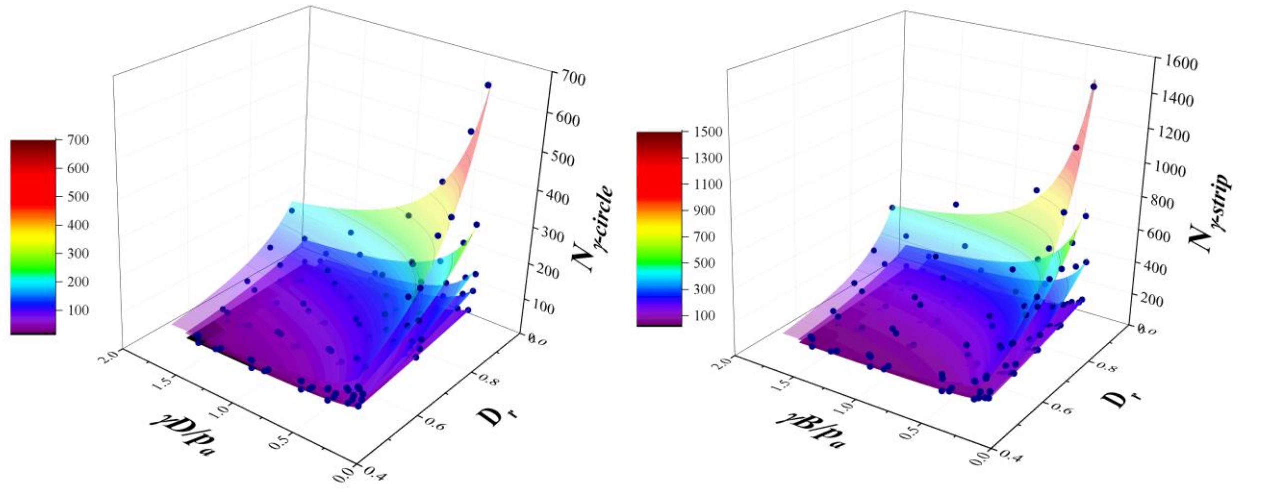

(a) (b)

Figure 13. 3D scatter (FEM results) and surface (fitted function) plots of $\gamma D/p_a$ or $\gamma B/p_a$, D_r and N_γ at different ϕ_{cr} (a) circular footing, (b) strip footing

5.1. Prediction of N_γ

The principal objective of this research is to aid in the evolution of a distinct, reliable, and standardized methodology to evaluate the ultimate bearing capacity of footings under vertical loads on sand substrates. The findings of the current investigation have been modeled utilizing a nonlinear surface fitting function. A unique surface is computed for each specific ϕ_{cr} value.

The following equation has been proposed that can predict bearing capacity factors of both circular and strip footings:

$$N_{\gamma-circle} = \frac{13.5+A*(\gamma D/p_a)^{-0.84}}{C+ {D_r}^{-0.84}} \tag{5}$$

$$N_{\gamma-strip} = \frac{69.6+A*(\gamma D/p_a)^{-1.3}}{C+ {D_r}^{-1.3}} \tag{6}$$

where A and C are parameters as a function of ϕ_{cr}.

$$A = \begin{cases} 9.78 \times 10^3 (\sin\phi_{cr})^{6.725/\sin\phi_{cr}} + 13.65\,, & for\ circular\ footing \\ 1.41 \times 10^8 \sin{\phi_{cr}}^{47.3\sin\phi_{cr}}\,, & for\ strip\ footing \end{cases} \tag{6.1}$$

$$C = \begin{cases} \frac{1.94}{\sin\phi_{cr}} - 4.31\,, & for\ circular\ footing \\ \frac{1}{-343(\sin\phi_{cr}-0.582)^2-1.024}\,, & for\ strip\ footing \end{cases} \tag{6.2}$$

The functions under consideration are shown in Figure 13, in conjunction with the results derived from the Finite Element Method (FEM). The regression's coefficient of determination (R^2) ranges approximately from 95% to 99%. After evaluating the parameter ranges, it can be seen that the proposed method demonstrates validity, albeit with certain constraints, within the specified ranges of D_r, $\gamma D/p_a$ or $\gamma B/p_a$, and ϕ_{cr}, as will be further elucidated.

5.2. Equivalent Mobilized Friction Angle ϕ_m

A concerted effort has been initiated to enhance the applicability of the predominant bearing capacity equations present in the contemporary literature and design standards. Although various equations are widely spread, the fitting process elucidates that, regardless of the theoretical framework used by Diaz-Segura [9] to define N_γ, the optimal fit is achieved with an expression of the following form.

$$N_{\gamma-strip} = \left[AN_q + B\right] tan(C\phi); \tag{7}$$

$$N_q = tan^2\left(\frac{\pi}{4}+\frac{\phi}{2}\right) exp(\pi \tan\phi) \tag{7.1}$$

where A, B, and C are fitting parameters. The average values for $N_{\gamma\text{-strip}}$, derived from approximately 60 methods, were utilized to fit the parameters for equal ϕ_p, resulting in a R^2 =0.99, with A = 1, B = 4.17, and C = 1.44.

The aforementioned equation was employed to apply $N_{\gamma\text{-strip}}$ values from the currently proposed methodology to determine the equivalent mobilized friction angle. The mobilized friction angle ϕ_m was subsequently plotted in relation to D_r and ϕ_{cr}, as shown in Figure 14. A function can be derived through nonlinear regression analysis to determine ϕ_m.

$$\phi_m = \phi_{cr} + \mathrm{A}\, D_r^{\,C-0.12\,ln\left(\frac{\gamma B}{p_a}\right)} + 1.19/\left(\frac{\gamma B}{p_a}\right) \tag{8}$$

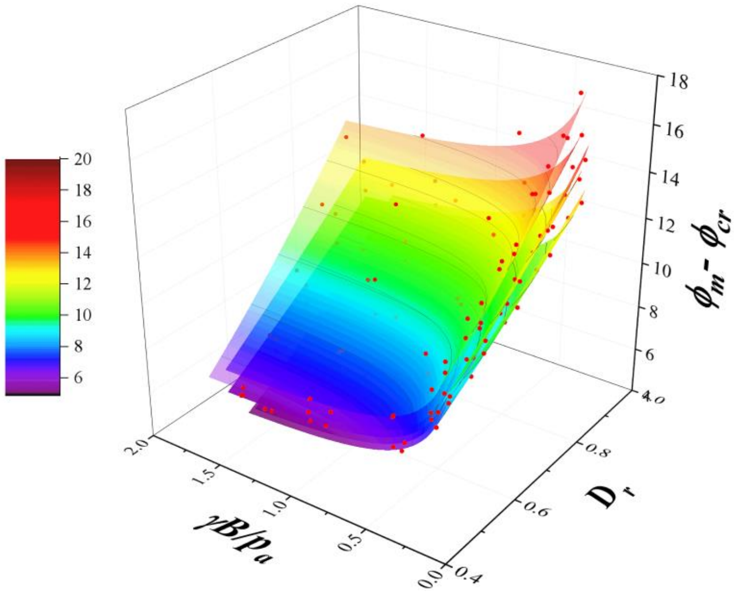

Figure 14. Variation of ϕ_m with $\gamma B/p_a$ and D_r

The derived equation yields a high accuracy range with R^2 values exceeding 0.98. The determined ϕ_m can be implemented in Equation 7 to calculate the bearing capacity factor $N_{\gamma\text{-strip}}$. The implementation of this function will facilitate ongoing research, and the development of design codes aimed at updating the current design methodology to rely on the stress level parameter $\gamma B/p_a$, the sand friction angle ϕ_{cr}, and the relative density of the sand D_r.

5.3. Correlation between $N_{\gamma\text{-circle}}$ and $N_{\gamma\text{-strip}}$

An effort has been made to establish a correlation between $N_{\gamma\text{-circle}}$ and $N_{\gamma\text{-strip}}$. The established correlation between these two factors is the ratio of $N_{\gamma\text{-circle}}$ / $N_{\gamma\text{-strip}}$, referred to as the shape factor. Numerous attempts have been made to determine the shape factor of a circular footing. Initial investigations based on 1-g model tests indicated a constant value of approximately 0.6 [63, 64]. Subsequent numerical research has revised this to be a function of the peak friction angle of the sand [65, 66]. According to centrifuge tests and the method of characteristics at D_r = 90%, a correlation of the shape factor with $\gamma D/p_a$ was proposed by Janabi et al. [2] and Zhu et al. [22]. Another FEM study by Chen et al. [51] also recommended a correlation with $\gamma D/p_a$. Although their investigation considered two types of sand and a wide range of footing diameters (1 m to 100 m) at different D_r values, the results were scattered. They suggested a constant value of approximately 0.4 for $D \leq 1$ m, while it converges to 1 for larger footings (D > 10 m). Other studies have indicated that the shape factor mainly depends on D_r, based on FEM [24] or 1-g tests [2]. From this concise summary, it can be inferred that certain studies have provided shape factor correlations based on 1-g tests, wherein $\gamma D/p_a$ values are minimal. Other studies used centrifuge tests at varying $\gamma D/p_a$, but D_r or sand type (ϕ_{cr}) remained constant throughout the study. Some numerical analyses explored the characteristic methods where the soil demonstrates plasticity and associated flow condition, which may not accurately depict sand behavior in medium to dense states.

In the present study, all parameters have been thoroughly examined. Utilizing Equations 5 and 6, $N_{\gamma\text{-circle}}$ and $N_{\gamma\text{-strip}}$ have been calculated at varied increments of $\gamma D/p_a$, D_r, and ϕ_{cr}. By plotting the calculated values at numerous D_r values with ϕ_{cr} set at 33° as an illustrative example, it is observed that the relationship exhibits pronounced nonlinearity as $\gamma D/p_a$ increases, as shown in Figure 15. The findings support the constant shape factors recommended by previous research based on 1-g model tests for minor values of $\gamma D/p_a$. Furthermore, the results corroborate the suggestion that the shape factor increases with an increase in $\gamma D/p_a$. However, the shape factor is influenced by both D_r and ϕ_{cr}. Further examination reveals that normalizing bearing capacity factors facilitates a distinctive correlation between $N_{\gamma\text{-circle}}$ and $N_{\gamma\text{-strip}}$.

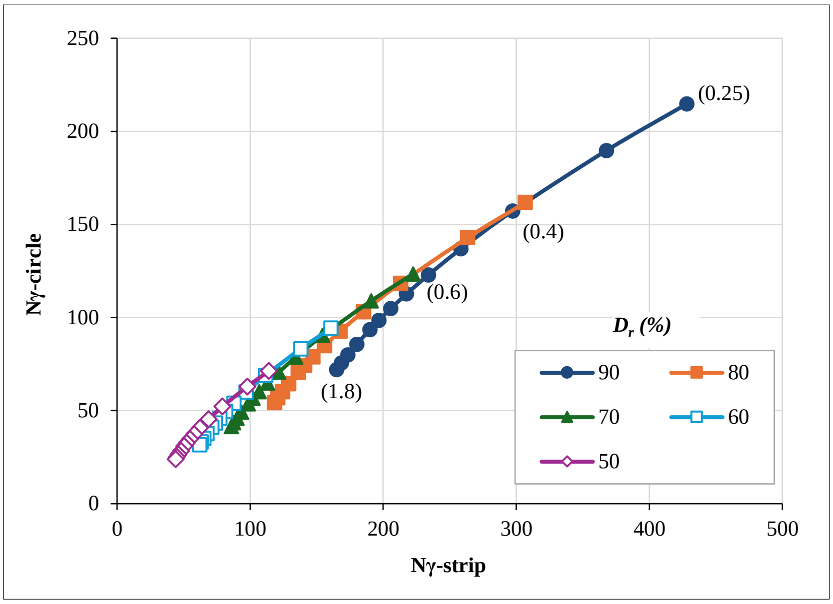

Figure 15. $N_{\gamma\text{-strip}}$ **versus** $N_{\gamma\text{-circle}}$ **for** ϕ_{cr} **= 33° at different** D_r **values (**$\gamma D/p_a$ **or** $\gamma B/p_a$ **values are in brackets)**

$$N^*_{\gamma-circle} = 0.558 \left(\frac{\gamma D}{p_a}\right)^{-0.417} \left(N^*_{\gamma-strip}\right)^{0.313} \tag{9}$$

where;

$$N^*_{\gamma-circle\ or\ strip} = \frac{N_{\gamma-circle\ or\ strip}}{N_{\gamma-circle\ or\ strip\ @0.25}} \tag{9.1}$$

The bearing capacity factor denoted as $N_{\gamma@0.25}$ pertains to circular or strip footings with specific values of D_r and ϕ_{cr}, with $\gamma D/p_a$ set at 0.25, representing the minimum value within the current study. The purpose of this correlation is to facilitate the prediction of $N_{\gamma\text{-circle}}$ from $N_{\gamma\text{-strip}}$. The subsequent relation holds true for $\gamma D/p_a$ = 0.25, universally applicable irrespective of D_r and ϕ_{cr}:

$$N_{\gamma-circle@0.25} = 1.47 \left(N_{\gamma-strip@0.25}\right)^{0.82} \tag{10}$$

Figure 16 shows three-dimensional plot of the normalized calculated values at different ϕ_{cr}. In addition, Equation 9 has been plotted as a fitted surface with accuracy R^2 = 0.999. This correlation can be used to predict bearing capacity of circular footing using Equation 6 or using Equations 7 and 8.

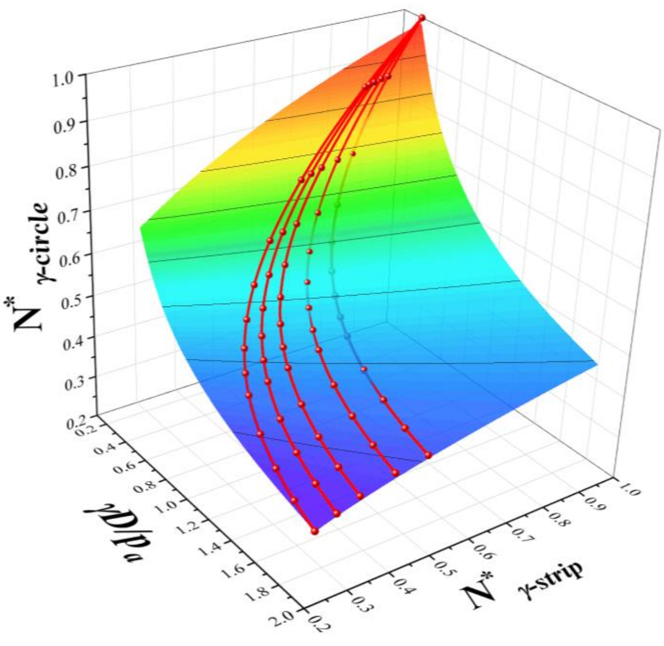

Figure 16. Three-dimensional correlation between $N_{\gamma\text{-strip}}$ **and** $N_{\gamma\text{-circle}}$

6. Comparison with Other Approaches

Based on the previous section discussion. The present study provides more than one approach that can predict the bearing capacity of both circular and strip footing. The following steps are to calculate both $N_{\gamma\text{-}strip}$ and $N_{\gamma\text{-}circle}$, at predefined values and within the ranges of $\gamma B/p_a$ or $\gamma D/p_a$ [0.25 – 1.85], D_r [50% – 90%], and ϕ_{cr} [30º - 35º].

- To calculate $N_{\gamma\text{-}strip}$: the direct approach ($PA1_s$) is to use Equation 6. The other approach ($PA2_s$) is to calculate the mobilized friction angle ϕ_m from Equation 8, then substitute it in Equation 7.
- To calculate $N_{\gamma\text{-}circle}$: the direct approach ($PA1_c$) is to use Equation 5. The other approach ($PA2_c$) is to use the correlation with $N_{\gamma\text{-}strip}$. This can be achieved using Equations 9 and 10 and using any of the aforementioned approaches to calculate $N_{\gamma\text{-}strip}$.

The proposed approaches have been subjected to scrutiny through various experimental centrifuge tests documented in the literature. A comprehensive set of centrifuge experiments was performed on circular and strip footings placed on dense sand the exhibits a relative density of 90%, as documented by Zhu et al. [22] and Zhu [56]. The footings used in these tests had diameters of 4.37 m, 5 m and 7 m and widths of 1.8 m and 2.4 m for circular and strip footings, respectively. The analysis revealed a variation in the critical friction angle ϕ_{cr} depending on the mean stress. However, the load-displacement curve from their centrifuge test with a diameter of 7 m, along with that of the strip footing, showed a behavioral similarity to other sands, where ϕ_{cr} ranged between 32˚ to 33˚. In addition, Toyoura sand had been studied extensively for circular and strip footings over a wide range of relative densities and stress parameter levels. As elaborated earlier, a critical friction angle ϕ_{cr} of 31.5˚ is adopted for Toyoura sand, as determined by modeling centrifuge experiments. The method used for the preparation of the sand exerts a notable influence on the results of centrifuge tests. The air pluviation technique, used by Ueno et al. [67], provides a homogeneous sand profile by depth. However, compacting sand causes deeper layers to be over compacted than shallower ones. This can be observed in results by Okamura et al. [7] where a larger footing diameter bearing capacity would correspond to a higher relative density than the average of 92%. The results by Ueno et al. [67] show more stable results on different footing sizes / stress level. The bearing capacity of the strip footing on the sand have been examined in a series of centrifuge tests by Ziccarelli et al. [59]. The tests were conducted on sand with an initial relative density = 95% and ϕ_{cr} of 32˚. However, they suggested an increase in D_r as a results of centrifuge gravity effect. Other centrifuge tests of circular footings on sand include Monterey 0/30 sand at an average relative density of 94 % and prototype footing diameters of 0.96 m and 1.91 m [60]. The critical friction angle ϕ_{cr} of Monterey 0/30 should be used to compare its findings with the currently recommended approach. A critical friction angle ϕ_{cr} value of 32.7˚ had been reported by Riemer et al. [68]. Inagi sand of ϕ_{cr} = 32˚ and with a relative density of about 80%, had been used in centrifuge tests to study the behavior of the circular surface footing under vertical centric load [54]. The stress level parameter was in the range of 0.14 to 0.43. The diameter of the footings ranged from 0.87 to 2.67 m. Centrifuge tests were performed using Leighton Buzzard sand of different fractions *C*, and *D* [61]. These fractions have d_{50} of 0.4 and 0.19, respectively. Using direct shear tests, they suggested ϕ_{cr} of 31.4˚, and 32˚ for the Leighton Buzzard sand fractions *C*, and *D*, respectively. Centrifuge tests were performed by Kokkali et al. [69] to study the behavior of square surface footings on Nevada sand of D_r = 45% and 90%. Square and circular footings of the same contact area on the same sand bed should behave identically [16]. A circular footing of an equivalent diameter on Nevada sand of ϕ_{cr} = 31˚can be compared well with those centrifuge tests. Centrifuge tests of circular footings of 2.4 m and 4.8 m diameter were conducted by White et al. [70]. UWA superfine sand of relative densities of 54 % and 78 % have been used. Sand has ϕ_{cr} of 32.2˚ as recommended by the same authors.

Tables 4 and 5 present the selected centrifuge tests along with their requisite design parameters such as D_r, $\gamma B/p_a$ or $\gamma D/p_a$, and ϕ_{cr} for the strip and circular footings, respectively. Furthermore, additional design methodologies cited in the literature [23, 24] are incorporated into both tables for comparative analysis. Figure 17 comprehensively presents the comparative results with alternative design methodologies. The precision of each design method is assessed based on the determination coefficient (R^2). The percentage error is shown, as well as the ratio of the difference between the bearing capacity factor of the experiment and that obtained from the design approach to that of the experiment. The findings demonstrate that the proposed method reliably estimates the bearing capacity of both the strip and circular footings within the preset parameter boundaries of the current investigation. For both types of footing, direct approaches yield more accurate predictions. Furthermore, applying the direct approach for strip footings to calculate the bearing capacity factor for circular footings results in commendable predictions. In contrast, the method based on the mobilized friction angle is less accurate compared to the direct approach. This corroborates the assertion by Diaz-Segura [9] that an error in the friction angle of ± 3º can lead to a variance greater than 250% in predicting N_γ. Despite the increased sensitivity associated with the friction angle, it provides a more accurate prediction of N_γ than methods from the existing literature. For circular footings, the comparative analysis adheres to the parameter confines mentioned previously. However, for strip footings, reliable predictions are achievable with D_r within the boundaries or > 90%, while maintaining the constraints of other parameters. The design approach proposed by Perkins and Madson [23] effectively predicts N_γ at low values, which correspond to large foundation sizes or low ϕ_{cr} for both strip and circular footings. However, it is significantly underestimated for larger values. This discrepancy may arise from inappropriate selection of critical friction angle values for various sands. Further investigation of their study indicates that they used high values for Toyoura sand, specifically 34º, whereas numerous authors advocate a value of 31.5º as discussed before. Similar miscalculations are observed for Nevada sand, they suggested ϕ_{cr} = 38 º while it was recommended as 31º by Kokkali et al. [69] and Hleibieh & Herle [71]. They also used ϕ_{cr} of 36 º for both Monterey 0/30 and Inagi sands while the values of 32.7 º and 32 º, respectively, were recommended by Jefferies and Been [12]. The other approach by Loukidis & Salgado [24] that has been used in the comparison shows high underprediction for strip footing case. However, the underprediction is less for circular footing cases. This could be due to the use of shape factor that decreases as D_r increases.

Table 4. Comparison of the proposed approach and available approaches for $N_{\gamma\text{-}strip}$ with experimental results (Actual)

Tests by	D_r%	ϕ_{cr} º	$\gamma D/p_a$	$N_{\gamma\text{-}strip}$								
				Exp.	PA1$_s$	*Er* %	PA2$_s$	*Er* %	[23]	*Er* %	[24]	*Er* %
Zhu et al. [22]	90	32.5	0.28	289.9	309.2	-7	292.7	-1	142.7	51	160.6	45
Zhu et al. [22]	90	32.5	0.37	262.1	250.8	4	233.7	11	124.1	53	145.9	44
Okamura et al. [8]	86	31.5	0.19	234.0	265.5	-13	262.5	-12	122.9	47	149.2	36
Okamura et al. [8]	86	31.5	0.25	209.0	210.8	-1	189.6	9	107.3	49	135.9	35
Okamura et al. [8]	86	31.5	0.33	200.0	174.6	13	151.5	24	94.5	53	124.6	38
Kimura et al. [72]	93	31.5	0.19	289.1	313.0	-8	322.5	-12	157.0	46	168.7	42
Kimura et al. [72]	93	31.5	0.28	262.5	227.9	13	205.9	22	128.8	51	146.3	44
Kimura et al. [72]	99	31.5	0.19	336.2	356.6	-6	383.0	-14	193.8	42	185.7	45
Kimura et al. [72]	99	31.5	0.29	305.9	259.3	15	240.9	21	157.7	48	159.5	48
Yamaguchi et al. [20]	90	31.5	0.19	283.4	291.0	-3	293.5	-4	141.0	50	160.0	44
Yamaguchi et al. [20]	90	31.5	0.25	249.9	230.7	8	210.3	16	122.7	51	144.9	42
Ziccarelli et al. [59]	100	32.0	0.26	370.1	350.0	5	349.8	5	191.6	48	180.3	51
Kimura et al. [72]	97	31.5	0.19	335.2	340.9	-2	360.3	-7	180.4	46	179.8	46
Kimura et al. [72]	97	31.5	0.29	303.1	247.5	18	227.4	25	147.0	52	154.7	49
Kimura et al. [72]	89	31.5	0.19	270.9	286.4	-6	288.4	-6	136.8	50	157.7	42
Kimura et al. [72]	89	31.5	0.28	246.7	207.2	16	184.2	25	112.2	55	137.2	44
Kimura et al. [72]	82	31.5	0.28	157.0	177.9	-13	155.9	1	89.5	43	123.0	22
Kimura et al. [72]	74	31.5	0.19	168.1	196.6	-17	187.6	-12	81.7	51	119.0	29
Kimura et al. [72]	74	31.5	0.27	136.0	148.2	-9	130.0	4	69.4	49	107.7	21
Kimura et al. [72]	74	31.5	0.36	122.7	122.0	1	105.5	14	60.8	50	99.3	19
Okahara [4]	88	31.5	0.47	140.3	149.8	-7	129.3	8	85.5	39	114.7	18
Okahara [4]	88	31.5	0.62	114.7	132.8	-16	115.2	0	75.2	34	105.3	8
Okahara [4]	74	31.5	0.46	91.0	107.9	-19	93.8	-3	55.0	40	93.5	-3
Okahara [4]	74	31.5	0.60	92.3	95.4	-3	84.2	9	48.7	47	87.0	6
Okahara [4]	58	31.5	0.44	70.9	71.3	-1	67.6	5	33.9	52	72.4	-2
Okahara [4]	58	31.5	0.60	57.1	62.3	-9	60.5	-6	29.9	48	68.3	-20

Table 5. Comparison of the proposed approach for $N_{\gamma\text{-}circle}$ with experimental results and available approaches

Tests by	D_r%	ϕ_{cr} º	$\gamma D/p_a$	$N_{\gamma\text{-}circle}$										
				Exp.	PA1$_c$	*Er* %	PA2$_c$$^{(1)}$	*Er* %	PA2$_c$$^{(2)}$	*Er* %	[23]	*Er* %	[24]	*Er* %
Kokkali et al. [69]	90	31	0.45	88.4	78.6	11	79.3	10	69.3	22	67.1	24	57.3	35
Zhu et al. [22]	90	32.5	0.27	166.6	169.2	-2	164.5	1	158.9	5	114.9	31	77.2	54
Zhu et al. [22]	90	32.5	0.67	113.4	96.5	15	94.4	17	91.6	19	74.2	35	67.8	40
Zhu et al. [22]	90	32.5	1.08	100.1	76.0	24	73.8	26	72.4	28	59.8	40	63.6	36
Kutter et al. [60]	95	32.7	0.32	191.8	186.9	3	181.8	5	177.9	7	129.8	32	80.4	58
Kusakabe [54]	80	32	0.28	112.9	110.1	2	108.5	4	100.2	11	74.0	34	65.9	42
Kusakabe [54]	80	32	0.44	74.8	83.7	-12	82.9	-11	76.6	-2	60.7	19	62.3	17
Okamura et al. [8]	100	31.5	0.25	159	159.6	0	154.8	3	150.7	5	135.1	15	72.0	55
Okamura et al. [8]	100	31.5	0.35	149	128.1	14	125.0	16	119.3	20	114.1	23	68.4	54
Ueno et al. [67]	70	31.5	0.24	85.6	87.7	-2	87.0	-2	79. 4	7	53.9	37	57.5	33
Ueno et al. [67]	70	31.5	0.48	54.4	57.0	-5	57.2	-5	51.9	5	39.8	27	53.3	2
Okamura et al. [7]	92	31.5	0.29	127	122.2	4	120.0	6	111.2	12	96.6	24	66.5	48
White et al. [70]	54	32.2	0.39	49.6	50.9	-3	50.8	-3	51.0	-3	31.4	37	53.6	-8
White et al. [70]	54	32.2	0.77	47.7	34.3	28	34.3	28	35.4	26	23.5	51	50.5	-6
White et al. [70]	78	32.2	0.40	79.7	88.8	-11	87.9	-10	81.6	-2	61.7	23	64.0	20
Jensen & Lehane [61]	82	31.4	0.40	71.6	80.0	-12	79.9	-11	71.3	0	60.3	16	58.5	18
Jensen & Lehane [61]	82	32	0.40	89.4	95.5	-7	94.3	-5	87.1	3	68.7	23	64.4	28

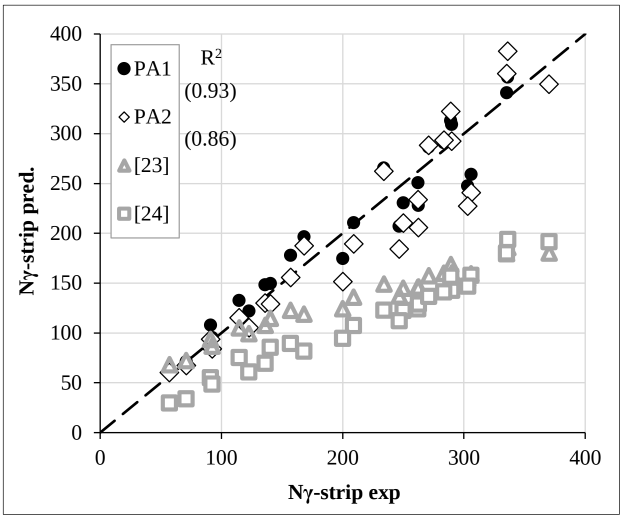

(a)

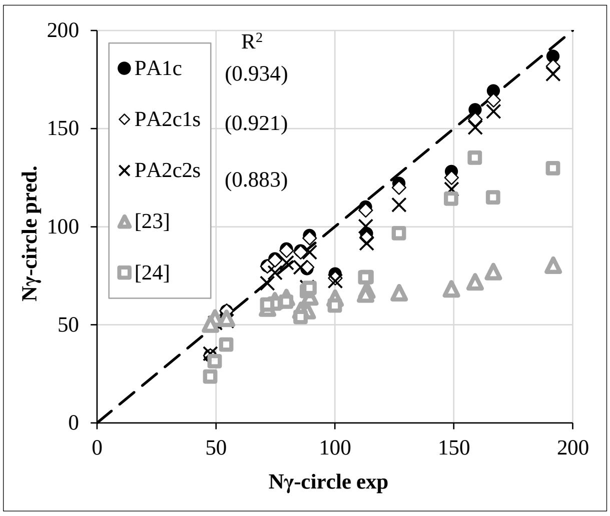

(b)

Figure 17. Comparison between the current approaches and experimental results and available approaches (a) strip, (b) circle

7. Conclusion

This study introduces an innovative design methodology for both strip and circular footings on sand surfaces. A three-Dimensional Finite Element Method (3-D FEM) has been developed. Sand is modeled using a hypoplastic sand model, which is an advanced framework capable of accurately predicting sand behavior under varying loading conditions governed by the void ratio. The model parameters have been selected on the basis of well-documented validation research in literature. The investigation concentrates on three primary variable parameters: the critical friction angle of the sand (ϕ_{cr} = 30˚–35˚), the relative densities of the sand (D_r = 50%-90%), and the footing size (1.5-10 m). FEM outcomes have been illustrated in three-dimensional graphs and adjusted using non-linear fitted surface functions. The results are described with respect to the bearing capacity factor N_γ for both strip and circular footings. Direct design approaches have been recommended for both types of footings, showing great agreement with experimental work from literature. An alternative approach for strip footing utilizes the mobilized friction angle ϕ_m. While minor errors in angle values can intensify the error in N_γ prediction, the present approach offers better predictions of N_γ than other methods in the literature. Furthermore, a correlation between $N_{\gamma\text{-strip}}$ and $N_{\gamma\text{-circe}}$ has been established rather than the shape factor. By employing $\gamma B/p_a$ or $\gamma D/p_a$ of 0.25 as a minimum criterion, along with the $N_{\gamma\text{-strip}}$ values from both mentioned approaches, $N_{\gamma\text{-circe}}$ can be predicted with notable precision.

It is imperative for future research to concentrate on conducting a greater number of comprehensively scaled experimental tests across a variety of sand types. The existing constraints on the parameters studied should be expanded. Given the challenge that lies in identifying calibrated sands through hypoplastic models, it is advisable to perform an inverse analysis on extant centrifuge tests to obtain additional calibrated sands, further extending the scope of the current study.

8. Declarations

8.1. Data Availability Statement

The data presented in this study are available on request from the corresponding author.

8.2. Funding and Acknowledgments

This project was funded by the Deanship of Scientific Research (DSR), King Abdulaziz University, Jeddah, under grant No. G:832-829-1441. The author, therefore, acknowledges with thanks DSR for technical and financial support.

8.3. Conflicts of Interest

The author declares no conflict of interest.

9. References

[1] Altaee, A., & Fellenius, B. H. (1995). Modeling the performance of the Molikpaq: Reply. Canadian Geotechnical Journal, 32(5), 924–926. doi:10.1139/t95-091.

[2] Janabi, F. H., Raja, R. A., Sakleshpur, V. A., Prezzi, M., & Salgado, R. (2023). Experimental Study of Shape and Depth Factors and Deformations of Footings in Sand. Journal of Geotechnical and Geoenvironmental Engineering, 149(2), 04022128. doi:10.1061/jggefk.gteng-10874.

[3] Bolton, M. D. (1986). The strength and dilatancy of sands. Geotechnique, 36(1), 65–78. doi:10.1680/geot.1986.36.1.65.

[4] Okahara, M. (1988). Centrifuge tests on scale effect of bearing capacity. Proceedings of the 42nd Annual Conference of the Japan Society of Civil Engineers, Tokyo, Japan.

[5] Altaee, A., & Fellenius, B. H. (1994). Physical modeling in sand. Canadian Geotechnical Journal, 31(3), 420–431. doi:10.1139/t94-049.

[6] Tatsuoka, F. (1991). Progressive failure and particle size effect in bearing capacity of a footing on sand. Proc. Geotechnical Engineering Congress, 10-12 June, 1991, Boulder, United States.

[7] Okamura, M., Takemura, J., & Kimura, T. (1997). Centrifuge Model Tests on Bearing Capacity and Deformation of Sand Layer Overlying Clay. Soils and Foundations, 37(1), 73–88. doi:10.3208/sandf.37.73.

[8] Okamura, M., Takemura, J., & Kimura, T. (1993). A Study on Bearing Capacities of Shallow Footings on Sand. Doboku Gakkai Ronbunshu, 1993(463), 85–94. doi:10.2208/jscej.1993.463_85.

[9] Diaz-Segura, E. G. (2013). Assessment of the range of variation of Nγ from 60 estimation methods for footings on sand. Canadian Geotechnical Journal, 50(7), 793–800. doi:10.1139/cgj-2012-0426.

[10] Santamarina, J. C., & Cho, G. C. (2001). Determination of Critical State Parameters in Sandy Soils - Simple Procedure. Geotechnical Testing Journal, 24(2), 185–192. doi:10.1520/gtj11338j.

[11] Sadrekarimi, A., & Olson, S. M. (2011). Critical state friction angle of sands. Géotechnique, 61(9), 771–783. doi:10.1680/geot.9.p.090.

[12] Jefferies, M., & Been, K. (2015). Soil liquefaction: a critical state approach. CRC Press, London, United Kingdom. doi:10.1201/b19114.

[13] Yang, J., & Luo, X. D. (2018). The critical state friction angle of granular materials: does it depend on grading? Acta Geotechnica, 13(3), 535–547. doi:10.1007/s11440-017-0581-x.

[14] Raja, R. A., Sakleshpur, V. A., Prezzi, M., & Salgado, R. (2023). Effect of Relative Density and Particle Morphology on the Bearing Capacity and Collapse Mechanism of Strip Footings in Sand. Journal of Geotechnical and Geoenvironmental Engineering, 149(8), 04023052. doi:10.1061/jggefk.gteng-11324.

[15] De Beer, E. E. (1965). Bearing capacity and settlement of shallow foundations on sand. Bearing Capacity and Settlement of Foundations: Proceedings of a Symposium, 5-6 April, Duke University, Durham, United Kingdom.

[16] Chakraborty, D., & Kumar, J. (2013). Dependency of Nγ on footing diameter for circular footings. Soils and Foundations, 53(1), 173–180. doi:10.1016/j.sandf.2012.12.013.

[17] Kumar, J., & Khatri, V. N. (2008). Effect of footing width on Ng. Canadian Geotechnical Journal, 45(12), 1673–1684. doi:10.1139/T08-113.

[18] Jahanandish, M., Veiskarami, M., & Ghahramani, A. (2010). Effect of Stress Level on the Bearing Capacity Factor, Nγ, by the ZEL Method. KSCE Journal of Civil Engineering, 14(5), 709–723. doi:10.1007/s12205-010-0866-1.

[19] Veiskarami, M., Jahanandish, M., & Ghahramani, A. (2010). Application of the Zel Method in the Prediction of Foundation Bearing Capacity Considering the Stress Level Effect. Soil Mechanics and Foundation Engineering, 47(3), 75–85. doi:10.1007/s11204-010-9092-6.

[20] Yamaguchi, H., Kimura, T., & Fuji-i, N. (1976). on the Influence of Progressive Failure on the Bearing Capacity of Shallow Foundations in Dense Sand. Soils and Foundations, 16(4), 11–22. doi:10.3208/sandf1972.16.4_11.

[21] Kamalzadeh, A., & Pender, M. J. (2023). Dilatancy Effects on Surface Foundations on Dry Sand. International Journal of Geomechanics, 23(3), 04022302. doi:10.1061/ijgnai.gmeng-7826.

[22] Zhu, F., Clark, J. I., & Phillips, R. (2001). Scale Effect of Strip and Circular Footings Resting on Dense Sand. Journal of Geotechnical and Geoenvironmental Engineering, 127(7), 613–621. doi:10.1061/(asce)1090-0241(2001)127:7(613).

[23] Perkins, S. W., & Madson, C. R. (2000). Bearing Capacity of Shallow Foundations on Sand: A Relative Density Approach. Journal of Geotechnical and Geoenvironmental Engineering, 126(6), 521–530. doi:10.1061/(asce)1090-0241(2000)126:6(521).

[24] Loukidis, D., & Salgado, R. (2011). Effect of relative density and stress level on the bearing capacity of footings on sand. Geotechnique, 61(2), 107–119. doi:10.1680/geot.8.P.150.3771.

[25] Ueno, K., Miura, K., & Maeda, Y. (1998). Prediction of ultimate bearing capacity of surface footings with regard to size effects. Soils and Foundations, 38(3), 165–178. doi:10.3208/sandf.38.3_165.

[26] Ueno, K., Miura, K., Kusakabe, O., & Nishimura, M. (2001). Reappraisal of Size Effect of Bearing Capacity from Plastic Solution. Journal of Geotechnical and Geoenvironmental Engineering, 127(3), 275–281. doi:10.1061/(asce)1090-0241(2001)127:3(275).

[27] Jitchaijaroen, W., Ranjan Kumar, D., Keawsawasvong, S., Wipulanusat, W., & Jamsawang, P. (2024). Hybrid artificial neural network models for bearing capacity evaluation of a strip footing on sand based on Bolton failure criterion. Transportation Geotechnics, 48. doi:10.1016/j.trgeo.2024.101347.

[28] Liu, Y., & Liang, Y. (2024). Integrated machine learning for modeling bearing capacity of shallow foundations. Scientific Reports, 14(1), 8319. doi:10.1038/s41598-024-58534-5.

[29] Alzabeebee, S., Alshkane, Y. M. A., & Keawsawasvong, S. (2023). New Model to Predict Bearing Capacity of Shallow Foundations Resting on Cohesionless Soil. Geotechnical and Geological Engineering, 41(6), 3531–3547. doi:10.1007/s10706-023-02472-y.

[30] Dehghanbanadaki, A., & Motamedi, S. (2024). Bearing capacity prediction of shallow foundation on sandy soils: a comparative study of analytical, FEM, and machine learning approaches. Multiscale and Multidisciplinary Modeling, Experiments and Design, 7(2), 1293–1310. doi:10.1007/s41939-023-00280-8.

[31] Lawal, A. I., & Kwon, S. (2023). Development of mathematically motivated hybrid soft computing models for improved predictions of ultimate bearing capacity of shallow foundations. Journal of Rock Mechanics and Geotechnical Engineering, 15(3), 747–759. doi:10.1016/j.jrmge.2022.04.005.

[32] Kumar, M., Kumar, V., Biswas, R., Samui, P., Kaloop, M. R., Alzara, M., & Yosri, A. M. (2022). Hybrid ELM and MARS-Based Prediction Model for Bearing Capacity of Shallow Foundation. Processes, 10(5), 1013. doi:10.3390/pr10051013.

[33] hahin, M. (2024). Progression of artificial intelligence/machine learning in geotechnical engineering. Machine Learning and Data Science in Geotechnics, 1(1), 1–5. doi:10.1108/mlag-10-2024-0010.

[34] Igoe, D., Zahedi, P., & Soltani-Jigheh, H. (2024). Predicting the Compression Capacity of Screw Piles in Sand Using Machine Learning Trained on Finite Element Analysis. Geotechnics, 4(3), 807–823. doi:10.3390/geotechnics4030042.

[35] Alipour, M. J., & Wu, W. (2024). A Simple Hypoplastic Model for Sand Under Cyclic Loading. Recent Geotechnical Research at BOKU, Springer Series in Geomechanics and Geoengineering, Springer, Cham, Switzerland. doi:10.1007/978-3-031-52159-1_1.

[36] Woodward, P. K., Nesnas, K., & Griffiths, D. V. (2000). Advanced numerical modelling of footings on granular soils. Proceedings of Sessions of Geo-Denver 2000 - Numerical Methods in Geotechnical Engineering, GSP 96, 284, 88–101. doi:10.1061/40502(284)7.

[37] Ramadan, M. I., & Meguid, M. (2020). Behavior of cantilever secant pile wall supporting excavation in sandy soil considering pile-pile interaction. Arabian Journal of Geosciences, 13(12). doi:10.1007/s12517-020-05483-8.

[38] Gudehus, G., Amorosi, A., Gens, A., Herle, I., Kolymbas, D., Mašín, D., Wood, D. M., Niemunis, A., Nova, R., Pastor, M., Tamagnini, C., & Viggiani, G. (2008). The soilmodels.info project. International Journal for Numerical and Analytical Methods in Geomechanics, 32(12), 1571–1572. doi:10.1002/nag.675.

[39] Mašín, D., & Duque, J. (2023). Excavation of Komořany Tunnel in Sand: A Case Study. International Journal of Geomechanics, 23(8). doi:10.1061/ijgnai.gmeng-8591.

[40] Qiu, G., & Grabe, J. (2012). Numerical investigation of bearing capacity due to spudcan penetration in sand overlying clay. Canadian Geotechnical Journal, 49(12), 1393–1407. doi:10.1139/T2012-085.

[41] Qiu, G., & Henke, S. (2011). Controlled installation of spudcan foundations on loose sand overlying weak clay. Marine Structures, 24(4), 528–550. doi:10.1016/j.marstruc.2011.06.005.

[42] Wichtmann, T., & Triantafyllidis, T. (2016). An experimental database for the development, calibration and verification of constitutive models for sand with focus to cyclic loading: part I—tests with monotonic loading and stress cycles. Acta Geotechnica, 11(4), 739–761. doi:10.1007/s11440-015-0402-z.

[43] Mašín, D. (2019). Modelling of Soil Behaviour with Hypoplasticity. In Springer Series in Geomechanics and Geoengineering. Springer International Publishing, Cham, Switzerland. doi:10.1007/978-3-030-03976-9.

[44] Ng, C. W. W., Boonyarak, T., & Mašín, D. (2013). Three-dimensional centrifuge and numerical modeling of the interaction between perpendicularly crossing tunnels. Canadian Geotechnical Journal, 50(9), 935–946. doi:10.1139/cgj-2012-0445.

[45] Wegener, D., & Herle, I. (2012). On stiffness at small strains in the context of hypoplasticity. Geotechnik, 35(4), 229–235. doi:10.1002/gete.201200006.

[46] Chow, S. H., Roy, A., Herduin, M., Heins, E., King, L., Bienen, B., ... & Cassidy, M. (2019). Characterisation of UWA superfine silica sand. GEO 18844, Centre for Offshore Foundation Systems, Crawley, Australia.

[47] Niemunis, A., & Herle, I. (1997). Hypoplastic model for cohesionless soils with elastic strain range. Mechanics of Cohesive-Frictional Materials, 2(4), 279–299. doi:10.1002/(SICI)1099-1484(199710)2:4<279::AID-CFM29>3.0.CO;2-8.

[48] Herle, I., & Gudehus, G. (1999). Determination of parameters of a hypoplastic constitutive model from properties of grain assemblies. Mechanics of Cohesive-Frictional Materials, 4(5), 461–486. doi:10.1002/(SICI)1099-1484(199909)4:5<461::AID-CFM71>3.0.CO;2-P.

[49] Yu, L. Q., Wang, L. Z., Guo, Z., Bhattacharya, S., Nikitas, G., Li, L. L., & Xing, Y. L. (2015). Long-term dynamic behavior of monopile supported offshore wind turbines in sand. Theoretical and Applied Mechanics Letters, 5(2), 80–84. doi:10.1016/j.taml.2015.02.003.

[50] Hong, Y., Koo, C. H., Zhou, C., Ng, C. W. W., & Wang, L. Z. (2017). Small Strain Path-Dependent Stiffness of Toyoura Sand: Laboratory Measurement and Numerical Implementation. International Journal of Geomechanics, 17(1), 1–10. doi:10.1061/(asce)gm.1943-5622.0000664.

[51] Chen, J., Dong, Y., & Whittle, A. J. (2020). Prediction and Evaluation of Size Effects for Surface Foundations on Sand. Journal of Geotechnical and Geoenvironmental Engineering, 146(5), 1–13. doi:10.1061/(asce)gt.1943-5606.0002237.

[52] Chen, Y., Zhao, W., Han, J., & Jia, P. (2019). A CEL study of bearing capacity and failure mechanism of strip footing resting on c-φ soils. Computers and Geotechnics, 111, 126–136. doi:10.1016/j.compgeo.2019.03.015.

[53] Morikage, A., Kusakabe, O., Yamaguchi, H., & Kobayanshi, T. (1990). Centrifuge model tests on bearing capacity of circular and rectangular footings on dry sand. Proceedings of the 25th Japan Annual Conference of Soil Mechanics and Foundation Engineering, Tokyo, Japan.

[54] Kusakabe, O. (1991). Experiment and analysis on the scale effect of Nγ for circular and rectangular footings. Proceedings of the International Conference Centrifuge, 13-14 June, 1991, Boulder, United States.

[55] Clark, J. I. (1998). The settlement and bearing capacity of very large foundations on strong soils: 1996 R.M. Hardy keynote address. Canadian Geotechnical Journal, 35(1), 131–145. doi:10.1139/t97-070.

[56] Zhu, F. (1998). Centrifuge modelling and numerical analysis of bearing capacity of ring foundations on sand. PhD Thesis, Memorial University of Newfoundland, St. John's, Canada.

[57] Govoni, L., Gourvenec, S., & Gottardi, G. (2010). Centrifuge modelling of circular shallow foundations on sand. International Journal of Physical Modelling in Geotechnics, 10(2), 35–46. doi:10.1680/ijpmg.2010.10.2.35.

[58] Cerato, A. B., & Lutenegger, A. J. (2007). Scale Effects of Shallow Foundation Bearing Capacity on Granular Material. Journal of Geotechnical and Geoenvironmental Engineering, 133(10), 1192–1202. doi:10.1061/(asce)1090-0241(2007)133:10(1192).

[59] Ziccarelli, M., Valore, C., Muscolino, S. R., & Fioravante, V. (2017). Centrifuge tests on strip footings on sand with a weak layer. Geotechnical Research, 4(1), 47–64. doi:10.1680/jgere.16.00021.

[60] Kutter, B. L., Abghari, A., & Cheney, J. A. (1989). Strength parameters for bearing capacity of sand. Journal of Geotechnical Engineering, 115(12), 1818–1819. doi:10.1061/(ASCE)0733-9410(1989)115:12(1818).

[61] Jensen, M. R., & Lehane, B. (2020). The effects of sand grading on the bearing capacity of surface foundations. 4th European Conference on Physical Modelling in Geotechnics. Lulea University of Technology, 6-8 September, 2020, Lulea, Sweden.

[62] De Beer, E. E. (1970). Experimental determination of the shape factors and the bearing capacity factors of sand. Geotechnique, 20(4), 387–411. doi:10.1680/geot.1970.20.4.387.

[63] Winterkorn, H. F., & Fang, H. Y. (1991). Soil technology and engineering properties of soils. Foundation engineering handbook, 88-143. Springer, Boston, United States. doi:10.1007/978-1-4615-3928-5_3.

[64] de Beer, E. E. (1970). Experimental Determination of the Shape Factors and the Bearing Capacity Factors of Sand. Géotechnique, 20(4), 387–411. doi:10.1680/geot.1970.20.4.387.

[65] Shafiqul Islam, M., Rokonuzzaman, M., & Sakai, T. (2017). Shape Effect of Square and Circular Footing under Vertical Loading: Experimental and Numerical Studies. International Journal of Geomechanics, 17(9), 06017014. doi:10.1061/(asce)gm.1943-5622.0000965.

[66] Lyamin, A. V., Salgado, R., Sloan, S. W., & Prezzi, M. (2007). Two- And three-dimensional bearing capacity of footings in sand. Geotechnique, 57(8), 647–662. doi:10.1680/geot.2007.57.8.647.

[67] Ueno, K., Nakatomi, T., & Mito, K. (1994). Influence of initial conditions on bearing characteristics of sand. International conference centrifuge 94, 31 August-2 September, 1994, Singapore.

[68] Riemer, M. F., Seed, R. B., Nicholson, P. G., & Jong, H. L. (1990). Steady state testing of loose sands: Limiting minimum density. Journal of Geotechnical Engineering, 116(2), 332–339. doi:10.1061/(ASCE)0733-9410(1990)116:2(332).

[69] Kokkali, P., Anastasopoulos, I., Abdoun, T., & Gazetas, G. (2015). Static and cyclic rocking on sand: Centrifuge versus reduced-scale LG experiments. Geotechnical Earthquake Engineering - Geotechnique Symposium in Print 2015, 64, 155–170. doi:10.1680/geot.14.P.064.

[70] White, D. J., Teh, K. L., Leung, C. F., & Chow, Y. K. (2008). A comparison of the bearing capacity of flat and conical circular foundations on sand. Geotechnique, 58(10), 781–792. doi:10.1680/geot.2008.3781.

[71] Hleibieh, J., & Herle, I. (2019). The performance of a hypoplastic constitutive model in predictions of centrifuge experiments under earthquake conditions. Soil Dynamics and Earthquake Engineering, 122, 310–317. doi:10.1016/j.soildyn.2018.10.031.

[72] Kimura, T., Kusakabe, O., & Saitoh, K. (1985). Geotechnical Model Tests of Bearing in a Centrifuge Capacity. Geotechnique, 35(1), 33–45. doi:10.1680/geot.1985.35.1.33.